Supporting Information

Sustainably Driven ZnO Nanocatalytic Paradigm for Assembling Novel Bis-Heteroaryl Indole Frameworks: Robust Cytotoxic Profiling against HCT116 and MCF-7 Cells

Parveen Kumar[1], Anurag Mishra[2], Gourav Kumar[1], Baldev[1], Prisha Bhatia[2], Sri Krishna Jayadev Magani[2], Meena Nemiwal[1*]*

[1]Department of Chemistry, Malaviya National Institute of Technology Jaipur, 302017, India

**Corresponding authors' Email: meena.chy@mnit.ac.in; jayadevmsk@snu.edu.in*

[2]Cancer Biology Lab, Department of Life Sciences, Shiv Nadar Institute of Eminence, Gautam Buddha Nagar, UP, India

Supporting Material

1. General Experiment Information

Experimental details: The ^{1}H, $^{13}C\{^{1}H\}$-NMR spectra were recorded using JEOL ECS-400 spectrometer (operating at 400 MHz for ^{1}H and 101 MHz for $^{13}C\{^{1}H\}$) in $CDCl_3$ and DMSO-d_6 solvent at room temperature. The proton resonances are annotated as: chemical shift (δ) relative to tetramethylsilane (δ 0.0) using the residual solvent signal as an internal standard or tetramethylsilane itself: chloroform-d (δ 7.26, singlet), DMSO-d_6 (δ 2.5 and 3.3 ppm), multiplicity (s, singlet; d, doublet; t, triplet; q, quartet; m, multiplet; br, broad), coupling constant (*J*, Hz). The chemical shifts of $^{13}C\{^{1}H\}$-NMR are reported in ppm relative to the central line of the triplet at 77.0 ppm for $CDCl_3$ and septet at 39.5 ppm for DMSO-d_6. HRMS spectra were recorded by using Q-TOF spectrometer in methanol solvent at room temperature.

General synthesis information: Reactions were run in screw capped glass vials (15 mL) stirred with Teflon®-coated magnetic stir bars. Experiments were monitored by thin layer chromatography (TLC). All products were purified by column layer chromatography using silica gel (230-400 mesh). TLC was prepared on silica gel plates and products were well examined under UV light. All reaction products were vacuum dried for several hours prior to being analyzed and weighted as well.

General procedure for catalytic reaction: In an oven-dried 15 mL glass vial, combine thiophene-2-carbaldehyde (*1.18 mmol or 112 µL*) and malononitrile (*1.10 mmol or 66 µL)* in ethanol (*1 mL*) along with ZnO nanocatalyst (*20 mol % or 18 mg*), and stir the mixture for 10 minutes. Subsequently, add indole (*1 mmol or 117 mg*) and continue stirring the reaction at room temperature for 2 hours. Monitor the progress of the reaction using thin layer chromatography (TLC). After completion, the reaction mixture was diluted with water and extracted with ethyl acetate (20 mL×3, 50 % V/V). The combined organic layer was washed with H_2O and brine, dried over anhydrous Na_2SO_4. After evaporation of the solvent the residue was adsorbed on the silica gel and the crude product was purified by column chromatography.

Materials: Derivatives of thiophene-2-carbaldehyde (98 % purity) and malononitrile (98 % purity) were purchased from BLD Pharmaceuticals and CDH, respectively. Chloroform-*d* (99.8% purity) and DMSO-d_6 used as an NMR solvent, were purchased from Sigma-Aldrich and Clear Synth respectively. Anhydrous zinc acetate dihydrate ($Zn(CH_3COO)_2{\cdot}2H_2O$), and sodium hydroxide were purchased from Loba Chemie and Qualikems respectively. All the solvents used were of analytical grade. Reactants, reagents, chemicals, and solvents available commercially within the country and used without purification.

2. Synthesis of Bis-heteroaryl Indole-Thiophene Scaffolds, Experimental Procedure for the Optimization Study, and Comparison with Prior Reports

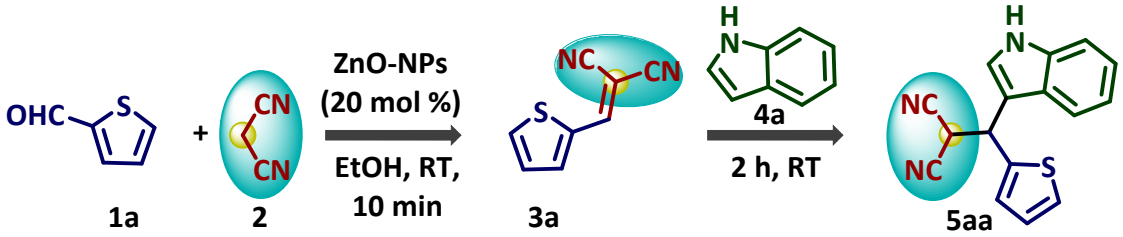

Bis-heteroaryl frameworks have garnered significant attention in medicinal chemistry due to their therapeutic relevance in treating various cancers and immunological disorders.[1] Nonetheless, the clinical utility of many existing agents is frequently limited by the emergence of resistance and adverse drug reactions, highlighting the urgent need for innovative pharmacological strategies. Motivated by the pivotal biological significance of indole-thiophene hybrids and the notable absence of synthetic methodologies leveraging aldehyde group activation of thiophene and furan ring, we initiated our investigation to explore this underdeveloped chemical space. Moreover, the comparison table with the closest previous reports has been also included to further substantiate the novelty (**Table S1**). The reaction was performed in warm air-dried glass vial of 15 mL capacity. For this methanol washed magnetic bead was put in reaction tube and then added 20 mol % (18 mg) of ZnO nanocatalyst, thiophene-2-carbaldehyde (1a) (*1.18 mmol or 112 µL*) and malononitrile (2) (*1.10 mmol or 66 µL)* and stir the reaction mixture for 10 minutes, and subsequently add indole (4a) (*1 mmol or 117 mg*). The reaction was stirred on magnetic stirrer with constant inspection of reaction on TLC and it was observed that maximum quantity of the reactant had been converted into product in 2 hours of reaction period. After completion, the reaction mixture was diluted with water and extracted with ethyl acetate. The product was separate out with the help of column chromatography method. The synthesis of the substituted fused thienopyridine products were examined by ^{1}H, $^{13}C\{^{1}H\}$-NMR, and HRMS characterization technique.

Table S1. Comparison of prior reports with current work

S. No.	Precursors	Catalyst	Reaction Conditions	Product	Ref.
1.	Benzaldehyde, Malononitrile, Indole	Copper (II) sulfonato Salen	KH_2PO_4, H_2O, 60 ˚C, 6 h	3-substituted Indole	[2]
2.	Benzaldehyde, Malononitrile, Indole	Zn(salphen) complex	*DIPEA*, DCM, RT, 6 h	3-substituted Indole	[3]
3.	Benzaldehyde,	--	$TBAF{\cdot}3H_2O$,	3-substituted	[4]

	Malononitrile, Indole		Solvent-free, 60 ˚C, 2 h	Indole	
4.	Benzaldehyde, Malononitrile, Indole	PEG-200	KH_2PO_4, H_2O, RT, 3 h	3-substituted Indole	[5]
5.	Benzaldehyde, pyrrolidine, Indole	RGO/ZnO	H_2O, RT, 0.5 h	3-substituted Indole	[6]
6.	Benzaldehyde, Malononitrile, Indole	L-Proline	Ethanol, RT, 48 h	3-substituted Indole	[7]
7.	Benzaldehyde, Malononitrile, Indole	$Cu(PPh_3)Cl$	H_2O, RT, 3 h	3-substituted Indole	[8]
8.	Benzaldehyde, Malononitrile, Indole	--	Micro droplet chemistry, *piperidine*, RT, 1 h	3-substituted Indole	[9]
9.	***Heteroaromatic aldehyde, Malononitrile, Indole***	***ZnO nanoparticles***	***EtOH, RT, 2 h***	***3-substituted Indole***	***Current work***

3. Recyclability and Hot-filteration Test:

The recyclability of ZnO nanoparticles was tested over five subsequent cycles. The catalyst was recovered after each cycle and reused with no substantial loss in catalytic performance, as indicated by consistent isolated yields (**Fig. S1-I**). Additionally, P-XRD analysis of the recycled catalyst confirms its crystalline nature is unchanged even after repeated usage (**Fig. S1-III, IV**). A hot-filteration test was also performed to evaluate the heterogeneous nature of catalyst, and found that there was no additional conversion take place in reaction after removal of the catalyst at an intermediate stage (1 h), indicating the lack of active species in reaction mixture (**Fig. S1-II**).

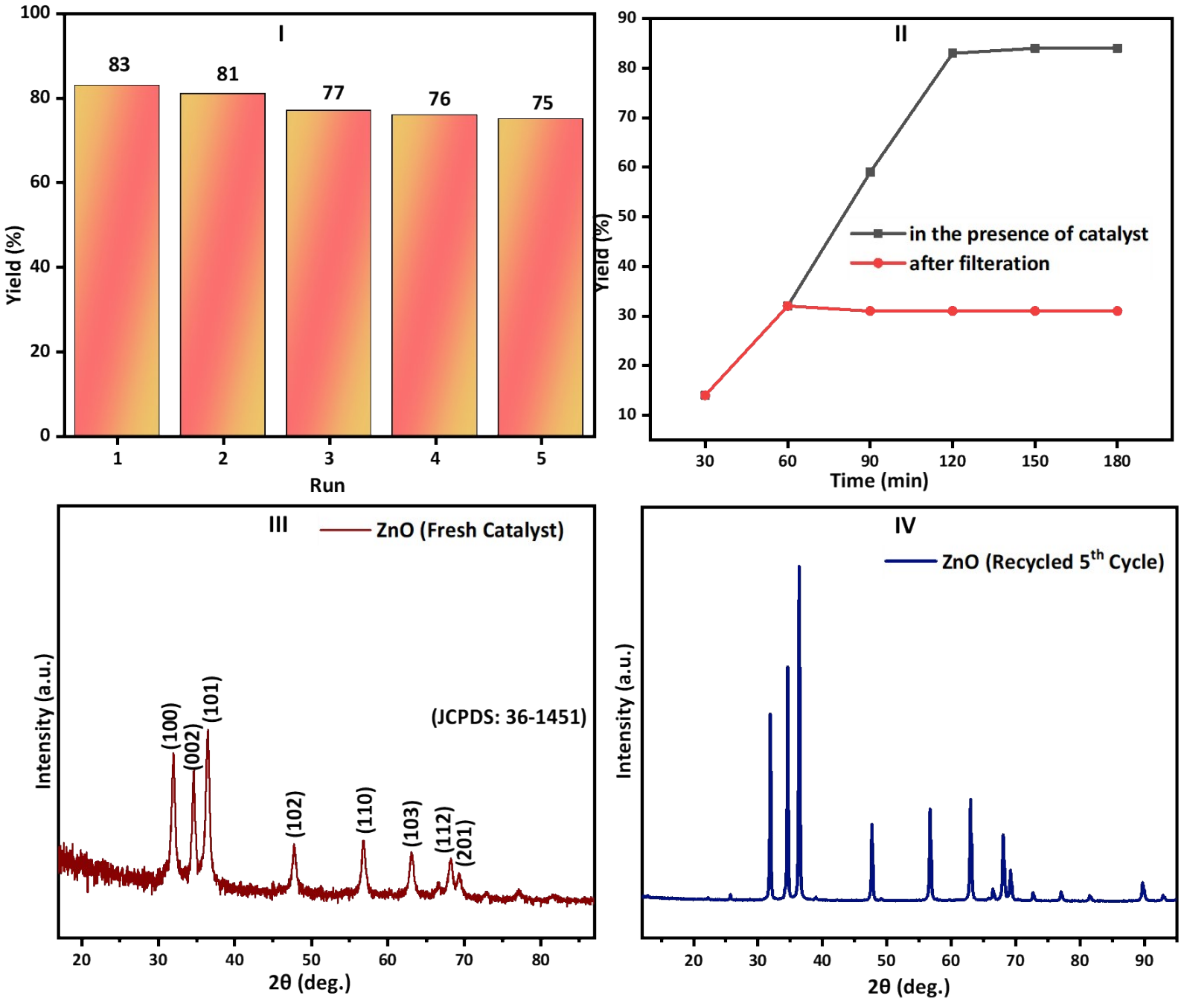

Figure S1. Recyclability study of the catalyst (I), hot-filteration test (II), P-XRD spectra of fresh and recycled ZnO nanoparticles (III, IV)

4. Anti-cancer Evaluation of Compound 5aa, 5ab, and 5ag against HCT116, MCF-7, and HEK-293 Cell Lines

Materials and methods

4.1 Materials: 5aa, 5ab, and 5ag, with molecular weights of 277.3450, 322.3420, and 327.4050 g/mol, respectively, were dissolved in DMSO, and a 10 mM stock solution was prepared. Further working dilutions were prepared to maintain the DMSO concentration below 0.5 % during experimental studies, as this concentration is not toxic to cells.

4.2 Cell lines, cell culture and media: HCT116, MCF7 and HEK293 were given as a kind gift from Dr. Sudip Sen, AIIMS DELHI and procured from ATCC. Dulbecco's modified Eagle medium (DMEM) with 10 % FBS and 1% Penstrep antibiotics was used to grow HCT116 (colon cancer), HEK293 (Human Embryonic Kidney), Reg-R-HCT (Regorafenib-resistant colon cancer) and MCF7 (Breast Cancer). Cells were incubated at 37 °C and 5% CO_2 in a humidified incubator.

4.3 Cell viability assay: The cell viability of the cells against 5aa, 5ab and 5ag was assessed using the MTT assay. The MTT is a colourimetric assay for determining cell viability and can be used to measure cytotoxicity. This assay is based on the cellular enzymes known as oxidoreductases, which are required to reduce the tetrazolium dye MTT to its insoluble, purple formazan crystals. Hence, the higher the intensity of purple colour formation, the greater the number of live cells. In 96-well cell culture plates, 1×10^4 cells/well of HCT116, MCF7 and HEK293 were allowed to grow for 24 h (HEK293 was used to test the cytotoxicity of these compounds in non-cancerous human cell lines). Cells were treated with compounds of the concentration gradient from 5 µM, 10µM, 15 µM, 20 µM, 25 µM and 30 µM for each compound for 48 h. Then, 50 µg/100 µL of MTT was added to the media post-treatment, and the cells were incubated in a CO_2 incubator for 2-3 h. The formazan crystals thus formed were resuspended in 100 µL DMSO. The absorbance of these cells was measured in an iMark Bio-Rad India microplate reader at 595 nm. Experiments were repeated three times. IC_{50} values were computed using the entire dose-response curve, with compound concentrations showing 50 % inhibition of cell number compared with cells with no compound cultured simultaneously.

4.4 Live-dead exclusion assay/Propidium Iodide staining (PI): The Propidium Iodide (PI) live-dead exclusion assay was conducted to validate the results of the MTT assay. PI is a dye that cannot permeate the intact plasma membrane of live cells. However, in late apoptotic or necrotic cells, the loss of membrane integrity allows PI to enter, bind with DNA, and exhibit red fluorescence.

To perform the assay, HCT116 cells (5 x 10^4 cells/well) were seeded in a 12-well plate and cultured for 24 hours. The cells were then treated with varying concentrations of compounds 5aa, 5ab, and 5ag for 48 hours. Post-treatment, the cells were stained with 10 µg/mL PI. They were then imaged using a Nikon TiE fluorescence microscope at 10x magnification, detecting the red emission wavelength.

4.5 Mitochondrial membrane potential loss by JC-1 staining: We looked for a hallmark of cell death due to apoptosis and membrane potential loss (MMP) to determine whether cell death occurred due to apoptosis. Mitochondrial Membrane Potential was evaluated by staining the compound-treated cells with JC-1 dye. The lipophilic, cationic JC-1 dye can enter mitochondria, accumulating and forming reversible complexes known as J-aggregates, which exhibit red fluorescence. The dye naturally exhibits green fluorescence. Hence, the JC-1 dye enters and builds up in the energized mitochondria, carrying a negative charge in healthy cells, and naturally forms red fluorescent J-aggregates. In unhealthy or apoptotic cells, the membrane becomes more permeable and loses its integrity, allowing JC-1 dye to leak from the mitochondria and exist as J-monomers, exhibiting green fluorescence. Twelve-well plates were seeded with 5×10^5 cells per well, and the plates were incubated for 24 h to allow the cells to adhere to the surface, after which they were treated with varying concentrations of the three compounds, as defined before. After 48 h of treatment, JC-1 dye was added to each well with a working concentration of 2 μM for 20 min. Then, the cells were examined by fluorescence microscopy with Nikon TiE Microscope 10× magnification using standard filters for TRITC and FITC. To verify the loss of MMP during apoptosis, 40 μM Carbonyl cyanide m-chlorophenyl hydrazine (CCCP) was taken as a positive control.

4.6 Reactive Oxygen Species (ROS) study: Using a Nikon TiE-fluorescence microscope with an emission wavelength of 530 nm, the dichlorofluorescein (DCFH) assay was used to quantify the cellular oxidative stress caused by drug response. DCFH-DA, a fluorescent probe, is utilised to find intracellular oxidative stress. In the presence of ROS, DCFH-DA is hydrolysed to DCFH and kept intracellularly. Fluorescent dichlorofluorescein, which fluoresces green, is produced when DCFH is oxidised. Cells are plated in 12-well plates at a density of 2.5×10^5 cells and allowed to grow in a CO_2 incubator for 24 h. Cells were treated with 5aa, 5ab and 5ag for 48 h. After that, cells were rinsed with 1X PBS, stained with 5 μM DFCH-DA, and incubated at 37 °C for 20 min. A Nikon TiE fluorescence microscope was used to image the cells using a FITC filter. 10× magnification was used for imaging HCT116.

4.7 Immunoblotting analysis: PCNA expression was studied in HCT cells upon administration of the compounds. Cells were treated at IC_{50} for 24-48 hours, followed by protein extraction and quantification using BCA. Equal amounts of total protein were resolved by SDS-PAGE and then transferred onto a PVDF membrane using wet transfer. The membrane was probed with a primary antibody targeting PCNA and a secondary antibody conjugated with an enzyme for detection, along with β-actin (housekeeping gene) as a control. The resulting bands were imaged, and the intensity of the bands for each sample was measured using ImageJ, which was further analysed. This allowed for the normalisation of PCNA levels against the loading control to determine the net protein expression induced by the compound treatments compared to the untreated control. Additionally, Paclitaxel was selected as a positive control for PI and ROS assays because it is a well-characterized apoptosis-inducing chemotherapeutic agent that produces classical morphological hallmarks of apoptosis, including nuclear fragmentation, ROS generation and membrane blabbing. Although paclitaxel induces apoptosis primarily through microtubule stabilization- mediated mitotic arrest, both paclitaxel and the tested compounds converge on PARP cleavage during

the execution phase of apoptosis.[10] Flow cytometry analysis of intracellular ROS generation in treated cells is depicted in **Fig. S2**. The mean ± standard deviation values of experiments are provided in **Table S2**.

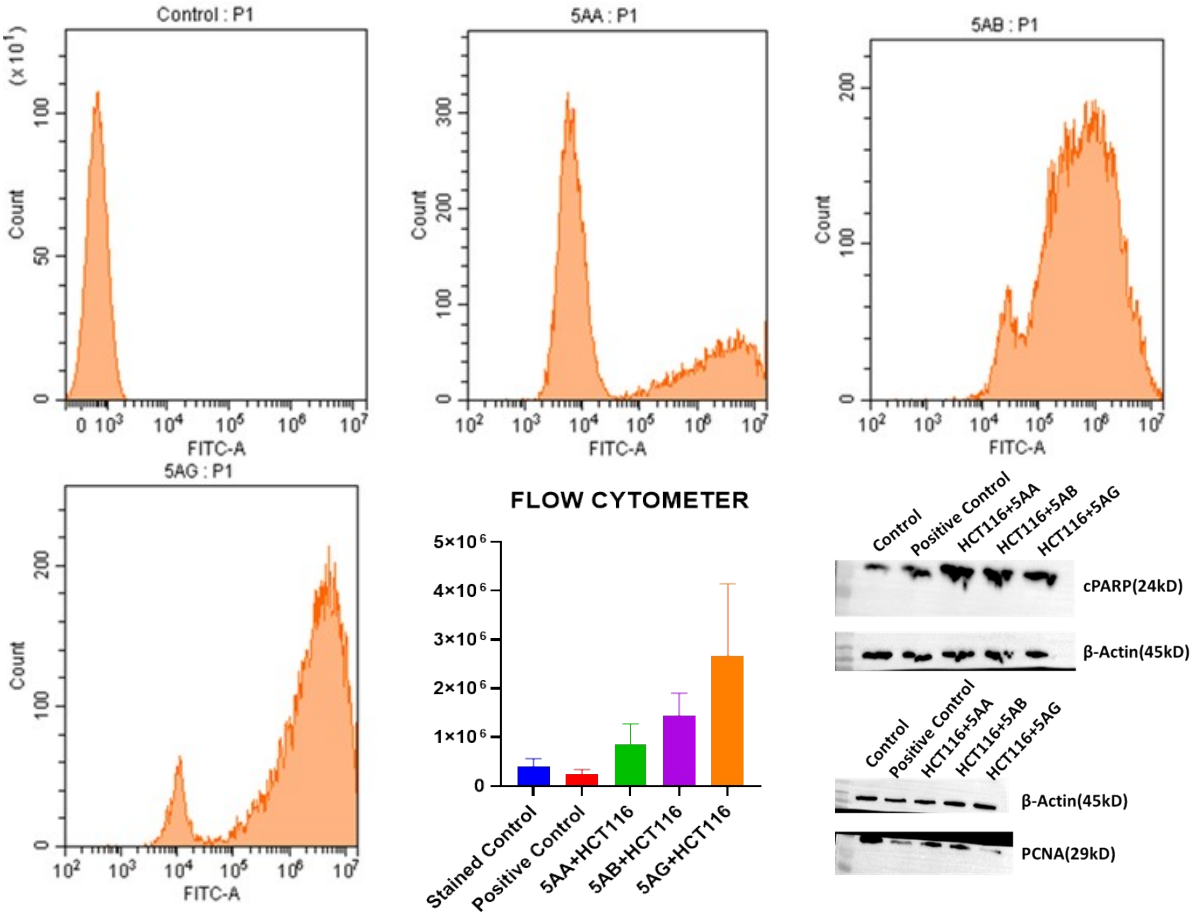

Figure S2. Flow cytometry analysis of intracellular ROS generation in treated cells and western blot image with positive control (Doxorubicin was used at 1.2 µM for 24 h)

Table S2. Calculation of mean ± SEM

	SEM Calculator from Confidence Interval					
	Uses: SEM when CI = x ± t×SEM					
	Mean (x)	**CI**	**t value**	**SEM**		
HCT116 5AA	8.07	9.631	4.303	**0.36**	**IC50**	**8.07 ±0.36**
HCT116 5AB	7.89	8.899	4.303	**0.23**	**IC50**	**7.889 ±0.23**
HCT116 5AG	5.08	6.495	4.303	**0.33**	**IC50**	**5.083 ±0.33**
MCF7 5AA	7.16	8.622	4.303	**0.34**	**IC50**	**7.158 ±0.34**
MCF7 5AB	7.99	8.913	4.303	**0.21**	**IC50**	**7.990 ±0.21**
MCF7 5AG	2.13	3.946	4.303	**0.42**	**IC50**	**2.126 ± 0.42**
HEK293 5AA	76.18	38.000	4.303	**-8.87**	**IC50**	**76.180 ± 8.87**
HEK293 5AB	10.08	10.730	4.303	**0.15**	**IC50**	**10.080 ±0.15**
HEK293 5AG	37.01	68.710	4.303	**7.37**	**IC50**	**37.010 ±7.37**

5. SC-XRD Data of 5aa Compound

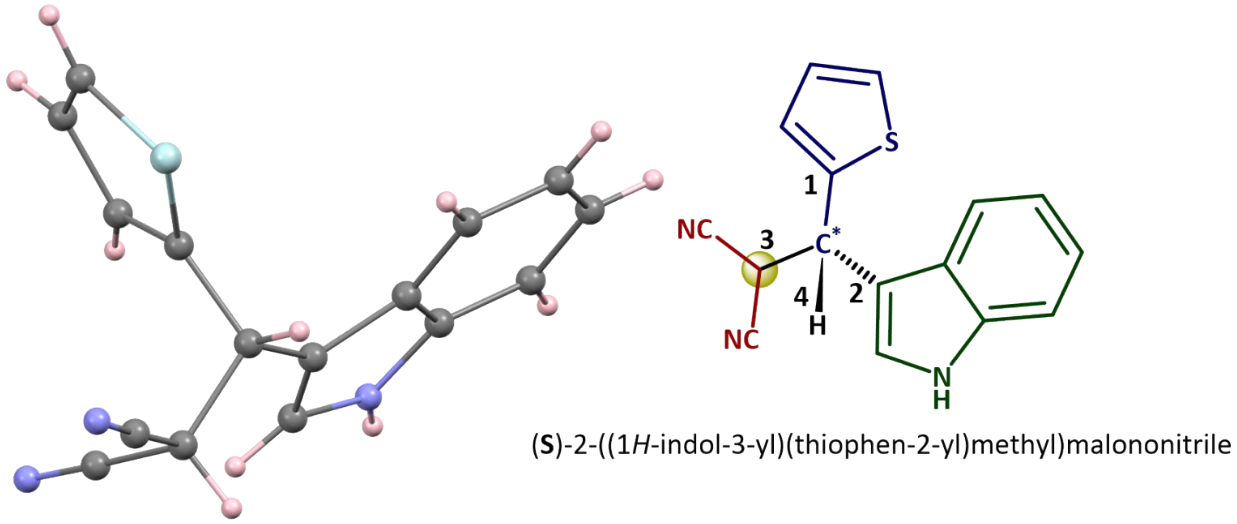

Figure S3. ORTEP diagram of compound **5aa (CCDC No 2487330)** along with stereochemistry

Table S3. Crystal data and structure refinement of compound **5aa**

Identification code	**Compound 5aa**
Empirical formula	$C_{16}H_{11}N_3OS$
Formula weight	277.352
Temperature/K	110.00
Crystal system	monoclinic
Space group	Cc
a/Å	14.3690(4)
b/Å	9.8569(3)
c/Å	11.8471(6)
α/°	90
β/°	126.062(1)
γ/°	90
Volume/Å^3	1356.42(9)
Z	4

ρ_{calc}g/cm^3	1.358
μ/mm^{-1}	0.230
F(000)	576.8
Crystal size/mm^3	0.269 × 0.186 × 0.179
Radiation	Mo Kα (λ = 0.71073)
2θ range for data collection/°	5.42 to 56.58
Index ranges	-19 ≤ h ≤ 19, -13 ≤ k ≤ 13, -15 ≤ l ≤ 15
Reflections collected	20727
Independent reflections	3355 [R_{int} = 0.0434, R_{sigma} = 0.0302]
Data/restraints/parameters	3355/12/190
Goodness-of-fit on F^2	1.038
Final R indexes [I>=2σ (I)]	R_1 = 0.0306, wR_2 = 0.0857
Final R indexes [all data]	R_1 = 0.0309, wR_2 = 0.0859
Largest diff. peak/hole / e Å^{-3}	0.49/-0.26
Flack parameter	0.024(15)

Table S4. Fractional Atomic Coordinates (×10^4) and Equivalent Isotropic Displacement Parameters (Å^2×10^3) for compound 102. U_{eq} is defined as 1/3 of the trace of the orthogonalised U_{IJ} tensor

Atom	*x*	*y*	*z*	U(eq)
C1	4611.6(11)	1830.7(13)	6234.0(14)	13.3(2)
C2	5245.4(12)	2224.4(14)	7645.9(15)	17.5(3)
C3	5672.2(13)	1221.1(16)	8655.5(15)	20.2(3)
C4	5487.8(13)	-165.1(16)	8283.9(16)	21.2(3)
C5	4884.9(13)	-579.2(14)	6911.3(16)	18.2(3)
C6	4449.4(11)	432.1(14)	5895.0(14)	14.9(3)

Atom	*x*	*y*	*z*	U(eq)
C7	3520.7(12)	1614.9(14)	3893.1(14)	16.9(3)
C8	4013.7(11)	2566.3(13)	4941.2(13)	13.0(2)
C9	4073.3(12)	4081.8(12)	4872.9(14)	12.8(2)
C10	5192.3(11)	4508.8(13)	5128.8(14)	13.5(2)
C11	5728.4(12)	3866.3(15)	4559.9(15)	18.3(2)
C12	6777.6(12)	4580.9(17)	5056.5(16)	21.5(3)
C13	7009.3(12)	5643.3(15)	5913.8(15)	19.9(3)
C14	3010.7(12)	4684.2(14)	3478.9(15)	16.8(3)
C15	3020.7(13)	6176.4(16)	3555.1(15)	20.0(3)
C16	2993.1(13)	4309.2(15)	2263.0(16)	20.2(3)
N1	3785.1(11)	336.8(12)	4467.1(13)	17.2(2)
N2	3066.2(12)	7339.0(14)	3633.6(14)	25.8(3)
N3	3000.8(14)	4024.7(15)	1327.5(15)	30.0(3)
S1	5976.3(3)	5854.0(3)	6185.6(4)	21.26(10)

Table S5. Anisotropic Displacement Parameters ($Å^2 \times 10^3$) for compound **5aa**. The Anisotropic displacement factor exponent takes the form: $-2\pi^2[h^2a^{*2}U_{11}+2hka^*b^*U_{12}+\ldots]$

Atom	U_{11}	U_{22}	U_{33}	U_{12}	U_{13}	U_{23}
C1	13.1(5)	10.9(5)	17.3(6)	-0.2(4)	9.8(5)	1.4(5)
C2	19.2(6)	13.6(6)	19.0(6)	-0.9(5)	10.9(5)	-0.5(5)
C3	21.7(7)	17.8(6)	17.6(6)	-0.6(5)	9.6(5)	1.1(5)
C4	19.5(6)	17.6(7)	22.8(7)	0.5(5)	10.4(5)	6.3(5)
C5	18.1(6)	11.6(6)	24.5(7)	-0.7(5)	12.4(6)	2.2(5)
C6	15.6(6)	11.4(6)	20.2(6)	-0.7(5)	11.9(5)	-0.7(5)

Atom	U_{11}	U_{22}	U_{33}	U_{12}	U_{13}	U_{23}
C7	22.2(6)	11.2(5)	17.8(6)	-2.0(5)	12.1(5)	-0.1(5)
C8	15.6(6)	9.6(5)	15.8(6)	0.2(5)	10.4(5)	1.3(4)
C9	15.3(6)	9.3(5)	15.2(6)	0.8(4)	9.7(5)	1.6(4)
C10	15.0(5)	10.2(5)	14.6(6)	-1.4(4)	8.2(5)	0.6(4)
C11	9.4(5)	19.7(6)	22.9(6)	-2.0(4)	7.9(5)	2.9(5)
C12	14.6(6)	26.2(7)	23.2(7)	-1.1(5)	10.8(5)	-0.7(5)
C13	15.3(6)	20.5(6)	20.3(7)	-4.2(5)	8.6(5)	1.9(5)
C14	14.6(6)	12.5(6)	22.6(6)	1.1(5)	10.6(5)	2.3(5)
C15	18.5(7)	16.4(7)	22.0(6)	3.1(5)	10.1(6)	5.0(5)
C16	18.4(7)	17.2(6)	18.2(6)	-1.4(5)	7.1(6)	3.3(5)
N1	24.7(6)	8.2(5)	20.8(6)	-2.4(4)	14.6(5)	-2.2(4)
N2	26.7(7)	17.8(6)	29.1(7)	4.4(5)	14.3(6)	5.7(5)
N3	34.6(8)	30.8(8)	17.7(6)	-5.3(6)	11.5(6)	0.2(5)
S1	20.73(17)	17.98(16)	23.56(17)	-4.24(14)	12.19(14)	-3.60(14)

Table S6. Bond lengths for compound **5aa**

Atom	Atom	Length/Å		Atom	Atom	Length/Å
C1	C2	1.4087(19)		C9	C10	1.5101(18)
C1	C6	1.4163(17)		C9	C14	1.5629(19)
C1	C8	1.4354(18)		C10	C11	1.435(2)
C2	C3	1.386(2)		C10	S1	1.7129(14)
C3	C4	1.412(2)		C11	C12	1.4391(19)
C4	C5	1.379(2)		C12	C13	1.357(2)
C5	C6	1.3956(19)		C13	S1	1.7066(16)

Atom	Atom	Length/Å		Atom	Atom	Length/Å
C6	N1	1.3714(18)		C14	C15	1.4732(19)
C7	C8	1.3739(19)		C14	C16	1.473(2)
C7	N1	1.3747(18)		C15	N2	1.148(2)
C8	C9	1.5011(17)		C16	N3	1.150(2)

Table S7. Bond angles for compound **5aa**

Atom	Atom	Atom	Angle/°		Atom	Atom	Atom	Angle/°
C6	C1	C2	119.22(12)		C14	C9	C8	112.57(11)
C8	C1	C2	133.66(12)		C14	C9	C10	111.63(11)
C8	C1	C6	107.09(12)		C11	C10	C9	125.81(12)
C3	C2	C1	118.46(13)		S1	C10	C9	121.79(10)
C4	C3	C2	120.99(14)		S1	C10	C11	112.39(10)
C5	C4	C3	121.75(14)		C12	C11	C10	108.35(13)
C6	C5	C4	117.21(13)		C13	C12	C11	114.84(14)
C5	C6	C1	122.36(13)		S1	C13	C12	112.19(11)
N1	C6	C1	107.17(12)		C15	C14	C9	110.26(11)
N1	C6	C5	130.41(13)		C16	C14	C9	112.44(12)
N1	C7	C8	109.46(12)		C16	C14	C15	107.72(12)
C7	C8	C1	106.61(12)		N2	C15	C14	177.77(17)
C9	C8	C1	122.88(12)		N3	C16	C14	178.70(17)
C9	C8	C7	130.24(12)		C7	N1	C6	109.66(12)
C10	C9	C8	110.75(11)		C13	S1	C10	92.22(7)

Table S8. Torsion angles for compound **5aa**

A	B	C	D	Angle/°	A	B	C	D	Angle/°
C1	C2	C3	C4	0.59(15)	C7	C8	C9	C10	-95.18(16)
C1	C6	C5	C4	0.18(15)	C7	C8	C9	C14	30.59(17)
C1	C6	N1	C7	-0.11(12)	C8	C1	C6	N1	-0.05(11)
C1	C8	C7	N1	-0.25(12)	C8	C9	C10	C11	42.66(14)
C1	C8	C9	C10	77.98(14)	C8	C9	C10	S1	-136.66(9)
C1	C8	C9	C14	-156.26(13)	C8	C9	C14	C15	171.22(12)
C2	C1	C6	C5	0.74(15)	C8	C9	C14	C16	-68.55(12)
C2	C1	C6	N1	178.39(13)	C9	C8	C7	N1	173.75(16)
C2	C1	C8	C7	-177.93(17)	C9	C10	C11	C12	-179.99(15)
C2	C1	C8	C9	7.52(18)	C9	C10	S1	C13	-179.99(11)
C2	C3	C4	C5	0.35(18)	C10	C9	C14	C15	-63.50(12)
C3	C2	C1	C6	-1.11(16)	C10	C9	C14	C16	56.74(12)
C3	C2	C1	C8	176.83(12)	C10	C11	C12	C13	0.31(14)
C3	C4	C5	C6	-0.73(17)	C10	S1	C13	C12	-0.43(10)
C4	C5	C6	N1	-176.86(12)	C11	C10	C9	C14	-83.62(15)
C5	C6	C1	C8	-177.69(14)	C11	C10	S1	C13	0.61(11)
C5	C6	N1	C7	177.28(16)	C11	C12	C13	S1	0.13(15)
C6	C1	C8	C7	0.18(12)	C12	C11	C10	S1	-0.62(13)
C6	C1	C8	C9	-174.37(10)	C14	C9	C10	S1	97.06(10)
C6	N1	C7	C8	0.23(13)					

Table S9. Hydrogen Atom Coordinates (Å×10^4) and Isotropic Displacement Parameters (Å^2×10^3) for compound **5aa**

Atom	*x*	*y*	*z*	U(eq)
H2	5377.2(12)	3155.9(14)	7900.2(15)	21.0(3)
H3	6095.1(13)	1469.9(16)	9611.8(15)	24.2(3)
H4	5786.8(13)	-830.3(16)	8998.1(16)	25.4(3)
H5	4700(20)	-1450(20)	6590(20)	27.3(4)
H7	3067.3(12)	1810.1(14)	2922.1(14)	20.2(3)
H9	4056(18)	4490(20)	5640(20)	19.3(4)
H11	5439.9(12)	3100.1(15)	3958.3(15)	22.0(3)
H12	7270.2(12)	4328.3(17)	4803.5(16)	25.9(3)
H13	7670.2(12)	6204.9(15)	6316.3(15)	23.8(3)
H14	2291.8(12)	4339.4(14)	3330.8(15)	20.1(3)
H1	3550(20)	-320(30)	4040(20)	25.7(4)

6. Chemical Synthesis and Spectroscopic Characterization Data

Table S10. Characterization data of representative compounds

S. No.	Structure of compound	Characterization data
1.	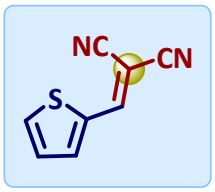	**2-(thiophen-2-ylmethylene)malononitrile (3a)** Yellow solid; Yield 89 %; M. P. 90-94 ˚C **^{1}H-NMR (400 MHz, $CDCl_3$)** δ 7.81 (s, 1H), 7.75-7.73 (m, 1H), 7.22-7.20 (m, 2H) ppm. **^{13}C{^{1}H}-NMR (101 MHz, $CDCl_3$)** δ 151.0, 138.1, 136.8, 135.2, 128.9, 113.7, 112.8, 78.2 ppm. **HRMS (ESI$^+$)** calculated for $C_8H_4N_2S$ $[M+H]^+$: 161.0168; found: 161.0170.
2.	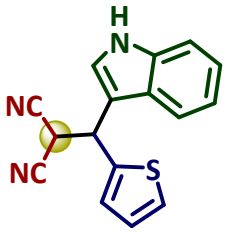	**2-((1H-indol-3-yl)(thiophen-2-yl)methyl)malononitrile (5aa)** Yellowish white solid; Yield 83 %; M. P. 110-114 ˚C **^{1}H-NMR (400 MHz, $CDCl_3$)** δ 8.25 (s, 1H, br), 7.40 (d, *J* = 8 Hz, 1H), 7.36-7.33 (m, 2H), 7.22 (dd, 1H), 7.18-7.16 (m, 2H), 7.10-7.05 (m, 1H), 6.95 (dd, 1H), 5.17 (d, *J* = 6 Hz, 1H), 4.37 (d, *J* = 6.4 Hz, 1H) ppm. **^{13}C{^{1}H}-NMR (101 MHz, $CDCl_3$)** δ 139.1, 135.1, 126.3, 126.0, 125.1, 124.5, 122.2, 121.9, 119.5, 117.3, 111.4, 111.0, 110.9, 110.7, 38.7, 29.9 ppm. **HRMS (ESI$^+$)** calculated for $C_{16}H_{11}N_3S$ $[M+H]^+$: 278.0747; found $[M+K]^+$: 316.0328.
3.	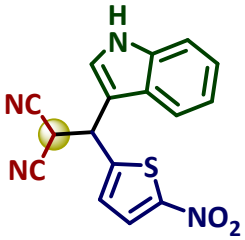	**2-((1H-indol-3-yl)(5-nitrothiophen-2-yl)methyl)malononitrile (5ab)** Brown semi-solid; Yield 86 % **^{1}H-NMR (400 MHz, $CDCl_3$)** δ 8.48 (s, 1H, br), 7.72 (d, *J* = 5.2 Hz, 1H), 7.36 (s, 1H), 7.22-7.17 (m, 2H), 7.14 (d, *J* = 4.4 Hz, 1H), 7.10-7.06 (m, 2H), 5.09 (d, *J* = 6.8 Hz, 1H), 4.39 (d, *J* = 6.0 Hz, 1H) ppm. **^{13}C{^{1}H}-NMR (101 MHz, $CDCl_3$)** δ 151.3, 148.3, 135.6, 128.2, 126.1, 124.6, 123.2, 122.3, 120.4, 117.4, 111.6, 111.0, 110.9, 110.0, 39.3, 29.5 ppm. **HRMS (ESI$^+$)** calculated for $C_{16}H_{10}N_4O_2S$ $[M+H]^+$: 323.0597; found: 323.0631.
4.		**2-((5-chlorothiophen-2-yl)(1H-indol-3-yl)methyl)malononitrile (5ac)** Brown liquid; Yield 84 % **^{1}H-NMR (400 MHz, $CDCl_3$)** δ 8.29 (s, 1H, br), 7.39-

	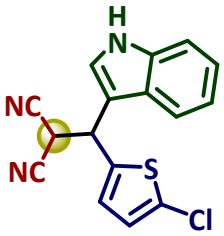	7.33 m, 2H), 7.22-7.18 (m, 2H), 7.11-7.07 (m, 1H), 6.95 (dd, 1H), 6.77 (d, J = 4 Hz, 1H), 5.03 (d, J = 6 Hz, 1H), 4.33 (d, J = 6 Hz, 1H) ppm. **^{13}C{^{1}H}-NMR (101 MHz, $CDCl_3$)** δ 137.4, 134.7, 129.6, 125.2, 125.0, 124.0, 122.0, 121.4, 119.3, 116.9, 110.5, 110.5, 110.4, 110.3, 38.5, 29.1 ppm. **HRMS (ESI$^+$)** calculated for $C_{16}H_{10}ClN_3S$ $[M+H]^+$: 312.0357; found: 312.0354.
5.	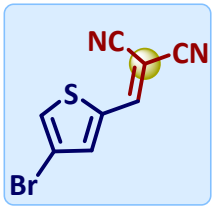	**2-((4-bromothiophen-2-yl)methylene)malononitrile (3d)** Yellow solid; Yield 91 %; M. P. 92-96 ˚C **^{1}H-NMR (400 MHz, DMSO-d_6)** δ 7.44 (s, 1H), 7.14 (s, 1H), 6.69 (s, 1H) ppm. **^{13}C{^{1}H}-NMR (101 MHz, DMSO-d_6)** δ 151.7, 140.1, 135.9, 134.7, 113.6, 112.8, 111.1, 77.9 ppm.
6.	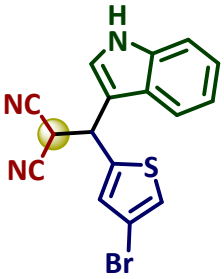	**2-((4-bromothiophen-2-yl)(1H-indol-3-yl)methyl)malononitrile (5ad)** Purple liquid; Yield 82 % **^{1}H-NMR (400 MHz, $CDCl_3$)** δ 8.36 (s, 1H, br), 7.37-7.33 (m, 2H), 7.31 (s, 1H), 7.20-7.16 (m, 1H), 7.10 (d, J = 1.6 Hz, 2H), 7.08 (s, 1H), 5.06 (d, J = 6.4 Hz, 1H), 4.31 (d, J = 6.4 Hz, 1H) ppm. **^{13}C{^{1}H}-NMR (101 MHz, $CDCl_3$)** δ 141.5, 136.0, 129.4, 125.3, 123.5,123.3, 122.9, 120.6, 118.1, 111.8, 111.7, 111.2, 109.9, 39.3, 30.5 ppm.
7.	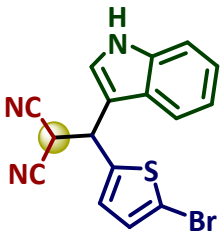	**2-((5-bromothiophen-2-yl)(1H-indol-3-yl)methyl)malononitrile (5ae)** Brown liquid; Yield 84 % **^{1}H-NMR (400 MHz, DMSO-d_6)** δ 11.32 (d, J = 2.8 Hz, 1H, br), 7.55-7.53 (m, 2H), 7.43-7.40 (m, 1H), 7.16 (s, 1H), 7.14-7.13 (m, 2H), 7.03-6.99 (m, 1H), 5.80 (d, J = 8 Hz, 1H), 5.59 (d, J = 8 Hz, 1H) ppm. **^{13}C{^{1}H}-NMR (101 MHz, DMSO-d_6)** δ 145.1, 136.5, 130.8, 128.2, 126.1, 123.9, 122.4, 119.7, 119.1, 114.1, 114.1, 112.4, 112.0, 111.8, 38.4, 30.2 ppm. **HRMS (ESI$^+$)** calculated for $C_{16}H_{10}BrN_3S$ $[M+H]^+$: 355.9852; found: 355.9848.
8.		**2-((5-ethylthiophen-2-yl)(1H-indol-3-yl)methyl)malononitrile (5af)** Brown liquid; Yield 77 %

	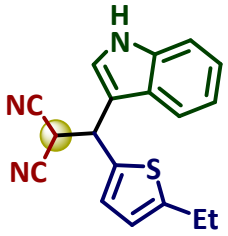	**^{1}H-NMR (400 MHz, $CDCl_3$)** δ 8.25 (s, 1H, br), 7.41 (d, *J* = 8.4 Hz, 1H), 7.39-7.34 (m, 2H), 7.21-7.17 (m, 1H), 7.11-7.07 (m, 1H), 6.97-6.96 (m, 1H), 6.62-6.61 (m, 1H), 5.10 (d, *J* = 6 Hz, 1H), 4.35 (d, *J* = 6.4 Hz, 1H), 2.72 (q, 2H), 1.20 (t, 3H) ppm. **^{13}C{^{1}H}-NMR (101 MHz, $CDCl_3$)** δ 147.4, 136.0, 135.0, 125.8, 124.6, 122.3, 122.0, 121.9, 119.3, 117.3, 111.3, 111.2, 111.1, 110.7, 38.9, 29.9, 22.4, 14.6 ppm.
9.	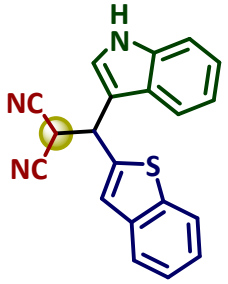	**2-(benzo[b]thiophen-2-yl(1H-indol-3-yl)methyl)malononitrile (5ag)** Yellow solid; Yield 86 %; M. P. 180-184 ˚C **^{1}H-NMR (400 MHz, $CDCl_3$)** δ 8.28 (s, 1H, br), 7.69-7.67 (m, 2H), 7.43 (d, *J* = 8 Hz, 1H), 7.39 (s, 1H), 7.38-7.37 (m, 1H), 7.34 (d, *J* = 8 Hz, 1H), 7.31-7.24 (m, 2H), 7.18-7.16 (m, 1H), 7.09-7.05 (m, 1H), 5.21 (d, *J* = 6 Hz, 1H), 4.46 (d, *J* = 6 Hz, 1H) ppm. **^{13}C{^{1}H}-NMR (101 MHz, $CDCl_3$)** δ 151.1, 142.4, 139.8, 136.7, 135.7, 133.8, 128.2, 125.1, 124.5, 123.7, 123.0, 122.2, 121.8, 121.3, 119.5, 117.3, 112.7, 110.8, 39.3, 29.3 ppm. **HRMS (ESI$^+$)** calculated for $C_{20}H_{13}N_3S$ $[M+H]^+$: 328.0903; found: 328.0899.
10.	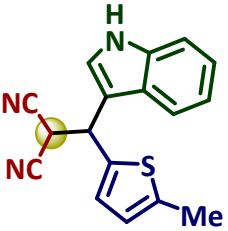	**2-((5-methylthiophen-2-yl)(1H-indol-3-yl)methyl)malononitrile (5ah)** Brown semi-solid; Yield 79 % **^{1}H-NMR (400 MHz, $CDCl_3$)** δ 8.24 (s, 1H, br), 7.42 (d, *J* = 8.0 Hz, 1H), 7.37-7.33 (m, 2H), 7.20-7.16 (m, 1H), 7.10-7.06 (m, 1H), 6.95-6.94 (m, 1H), 6.60-6.58 (m, 1H), 5.08 (d, *J* = 6.8 Hz, 1H), 4.35 (d, *J* = 6 Hz, 1H), 2.36 (s, 3H) ppm. **^{13}C{^{1}H}-NMR (101 MHz, $CDCl_3$)** δ 139.8, 136.4, 135.1, 126.0, 124.5, 124.3, 122.1, 121.8, 119.4, 117.3, 111.4, 111.1, 111.0, 110.7, 38.9, 29.9, 14.3 ppm. **HRMS (ESI$^+$)** calculated for $C_{17}H_{13}N_3S$ $[M+H]^+$: 292.0903; found: 292.0911.
11.	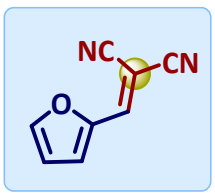	**2-(furan-2-ylmethylene)malononitrile (3h)**[11] Yellow solid; Yield 83 %; M. P. 70-74 ˚C **^{1}H-NMR (400 MHz, $CDCl_3$)** δ 7.74 (d, *J* = 2 Hz, 1H), 7.46 (s, 1H), 7.28 (d, *J* = 4 Hz, 1H), 6.66-6.65 (m, 1H) ppm. **^{13}C{^{1}H}-NMR (101 MHz, $CDCl_3$)** δ 148.7, 147.1,

		142.1, 122.7, 113.5, 112.9, 11.7, 76.4 ppm.
12.	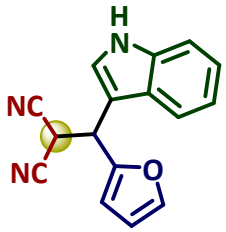	**2-(furan-2-yl(1H-indol-3-yl)methyl)malononitrile (5ah)** Brown liquid; Yield 78 % **^{1}H-NMR (400 MHz, $CDCl_3$)** δ 8.28 (s, 1H, br), 7.52-7.49 (m, 1H), 7.41 (t, 1H), 7.37 (d, *J* = 3.2 Hz, 1H), 7.33 (s, 1H), 7.21-7.19 (m, 1H), 7.12-7.08 (m, 1H), 6.31 (S, 2H), 4.99 (d, *J* = 6 Hz, 1H), 4.44 (d, *J* = 6 Hz, 1H) ppm. **^{13}C{^{1}H}-NMR (101 MHz, $CDCl_3$)** δ 148.8, 142.2, 135.0, 124.6, 122.8, 122.1, 119.5, 117.3, 111.0, 110.8, 110.8, 109.9, 108.7, 108.5, 37.4, 28.0 ppm. **HRMS (ESI^{+})** calculated for $C_{16}H_{11}N_3O$ $[M+H]^+$: 262.0975; found: 262.0972.

7. Characterization of Synthetic Intermediate Compound

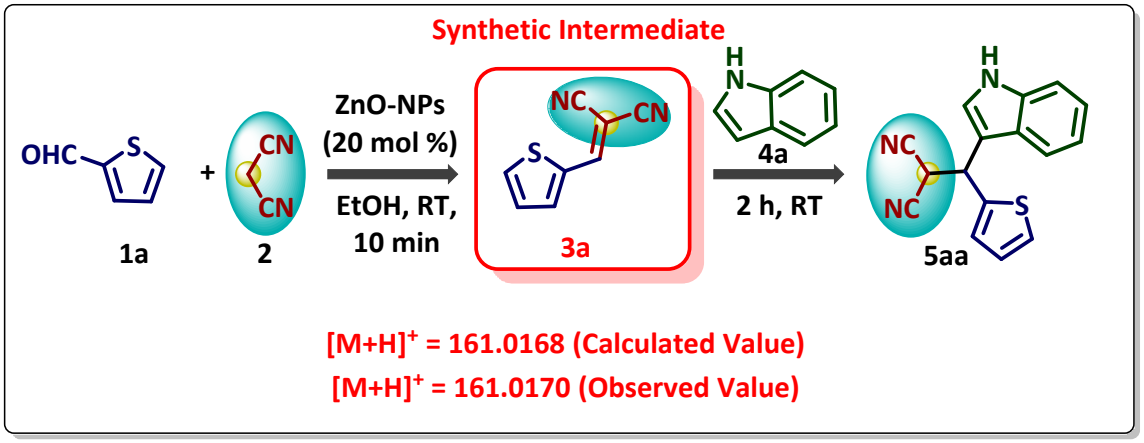

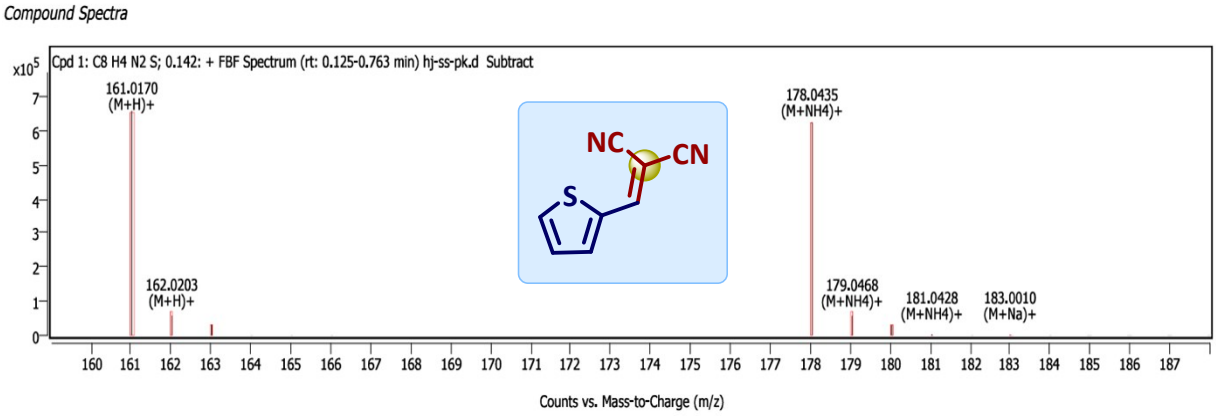

Figure S4: HRMS of synthetic intermediate compound (**3a**)

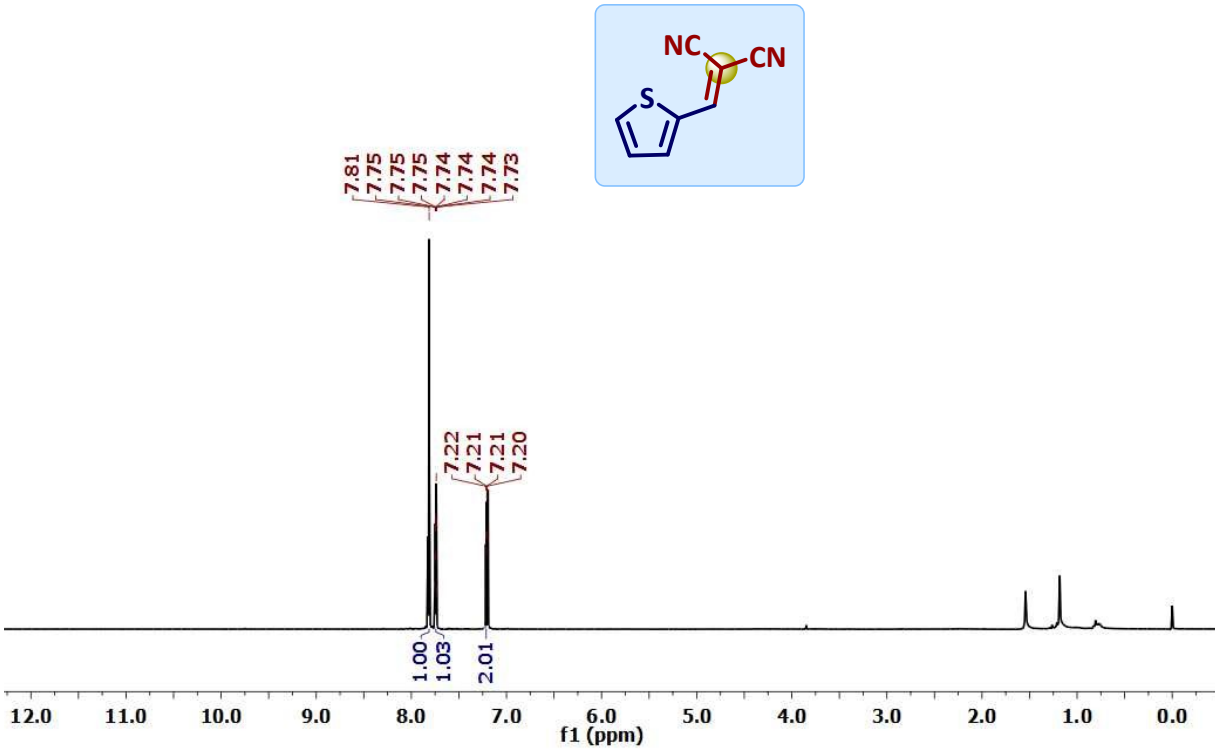

Figure S5: ^{1}H-NMR spectrum (400 MHz) in $CDCl_3$ of intermediate compound (**3a**)

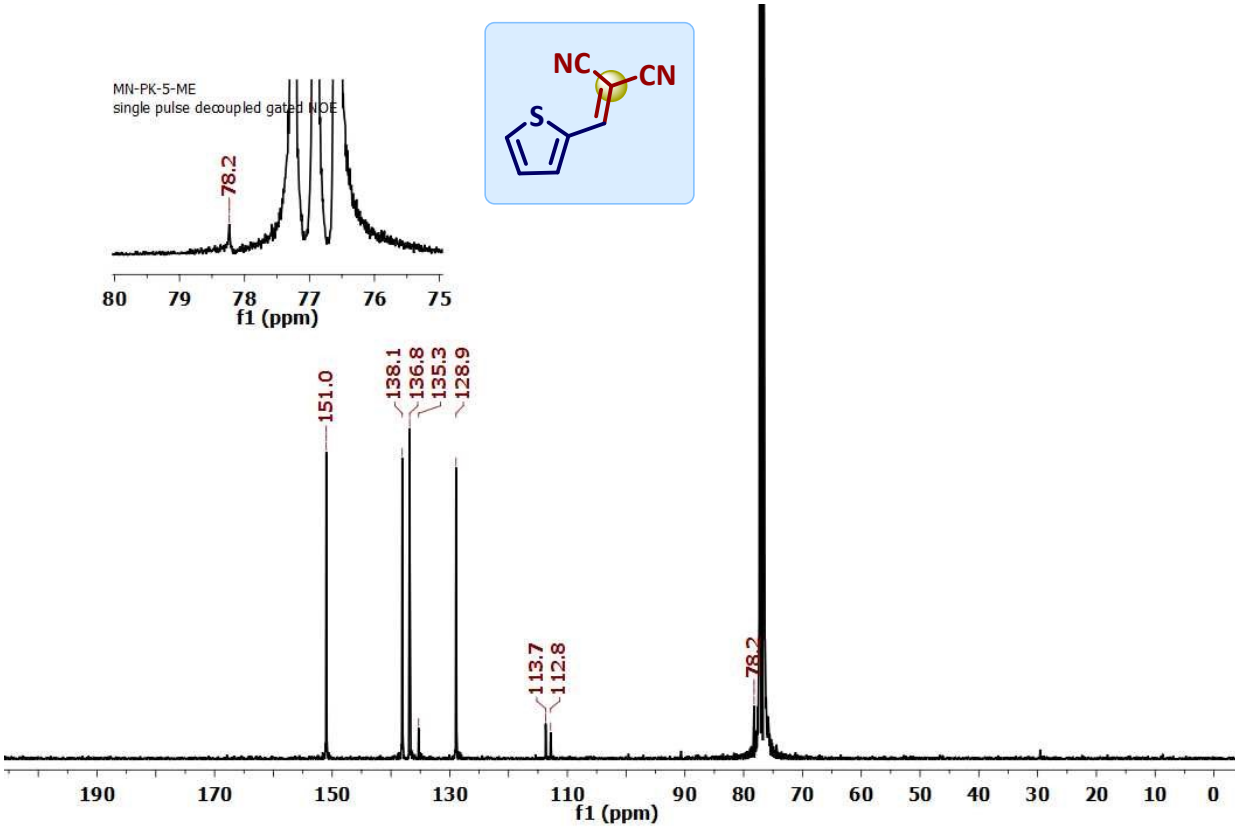

Figure S6: $^{13}C\{^{1}H\}$-NMR spectrum (101 MHz) in $CDCl_3$ of intermediate compound (**3a**)

8. ^{1}H and $^{13}C\{^{1}H\}$-NMR Spectra of Compounds

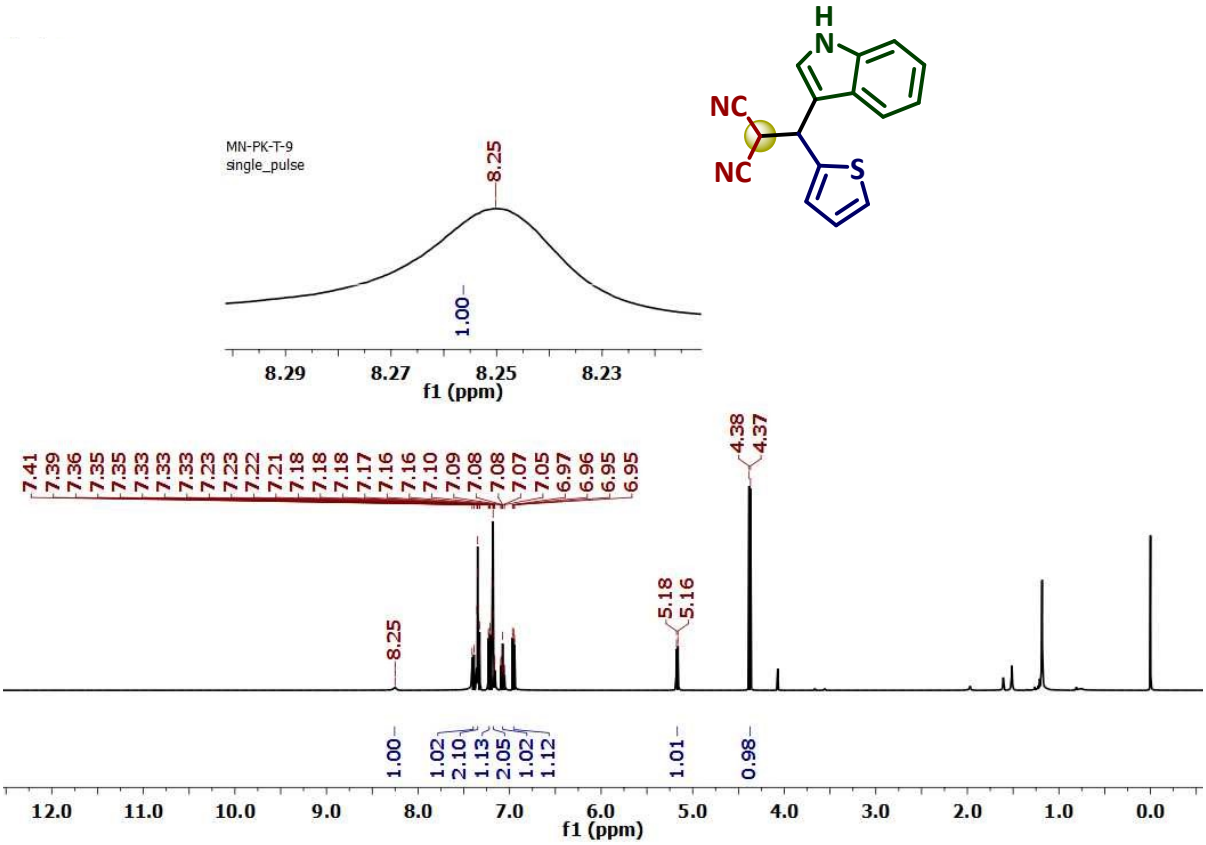

Figure S7: ^{1}H-NMR spectrum (400 MHz) in $CDCl_3$ of **5aa** compound

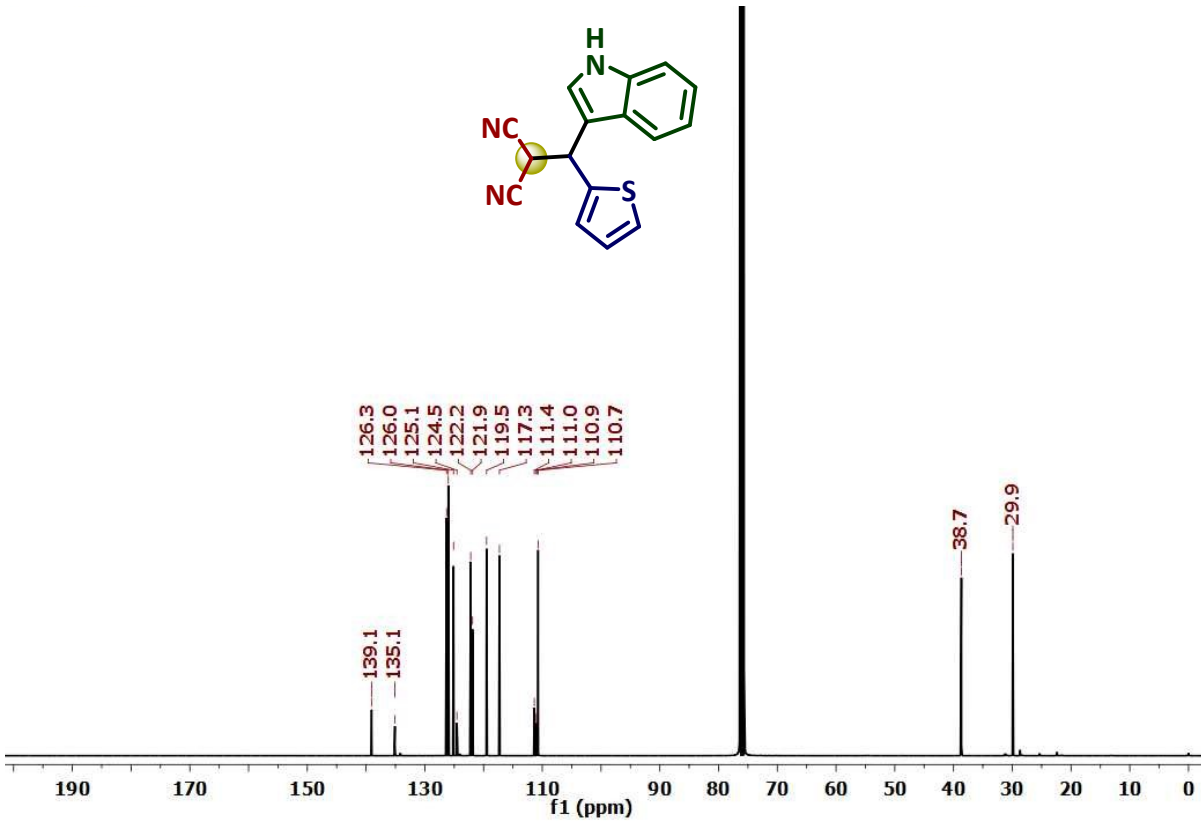

Figure S8: $^{13}C\{^{1}H\}$-NMR spectrum (101 MHz) in $CDCl_3$ of **5aa** compound

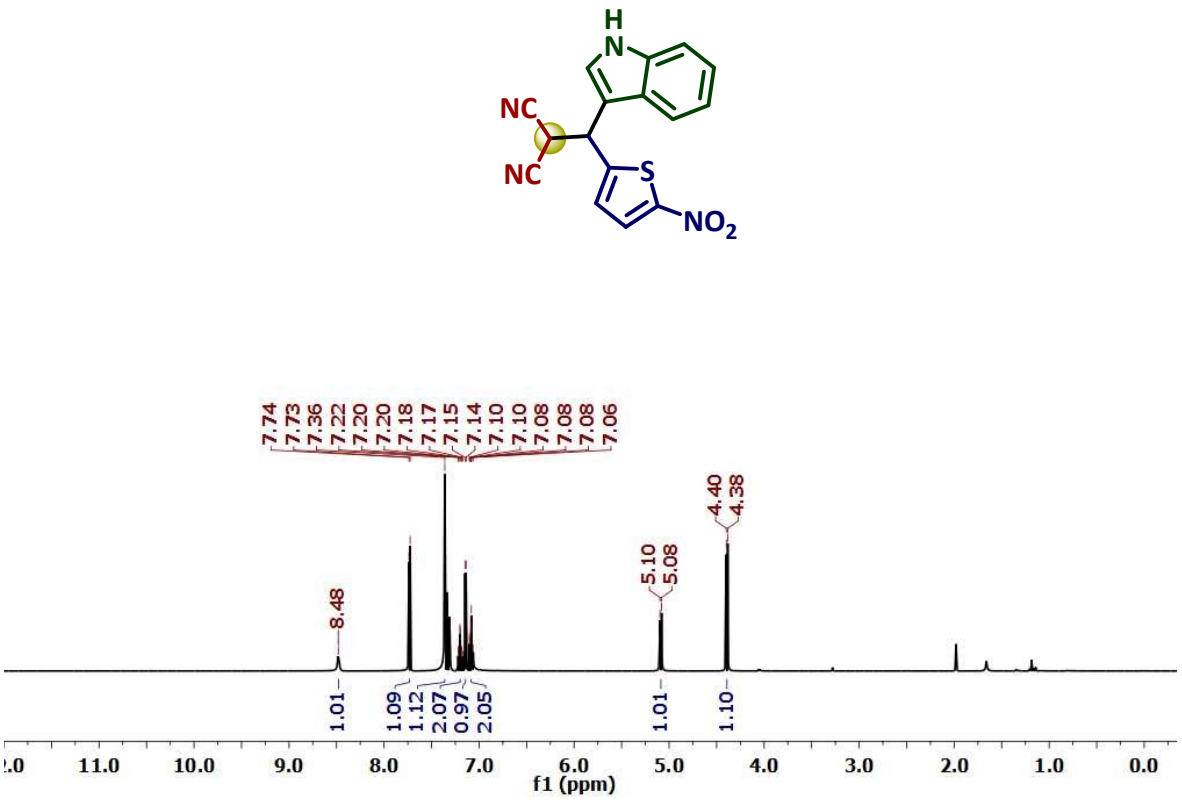

Figure S9: ^{1}H-NMR spectrum (400 MHz) in $CDCl_3$ of **5ab** compound

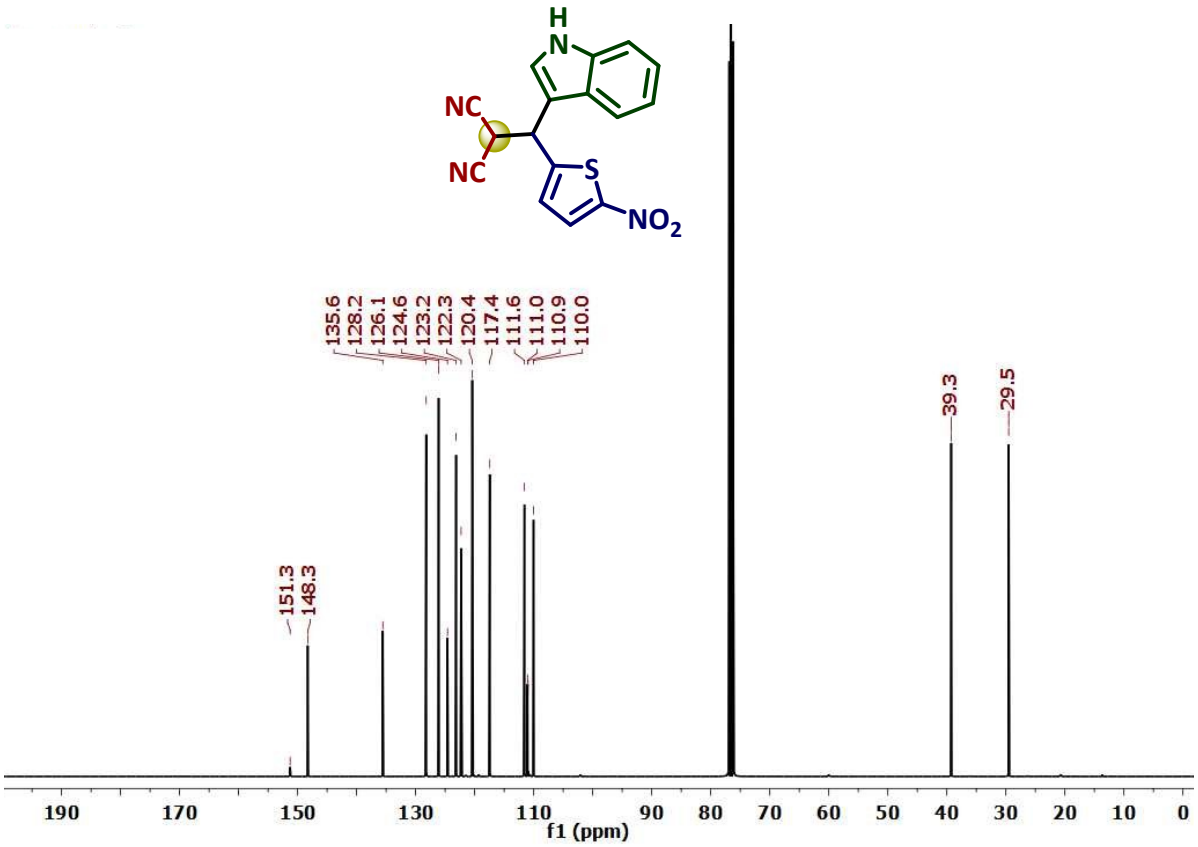

Figure S10: $^{13}C\{^{1}H\}$-NMR spectrum (101 MHz) in $CDCl_3$ of **5ab** compound

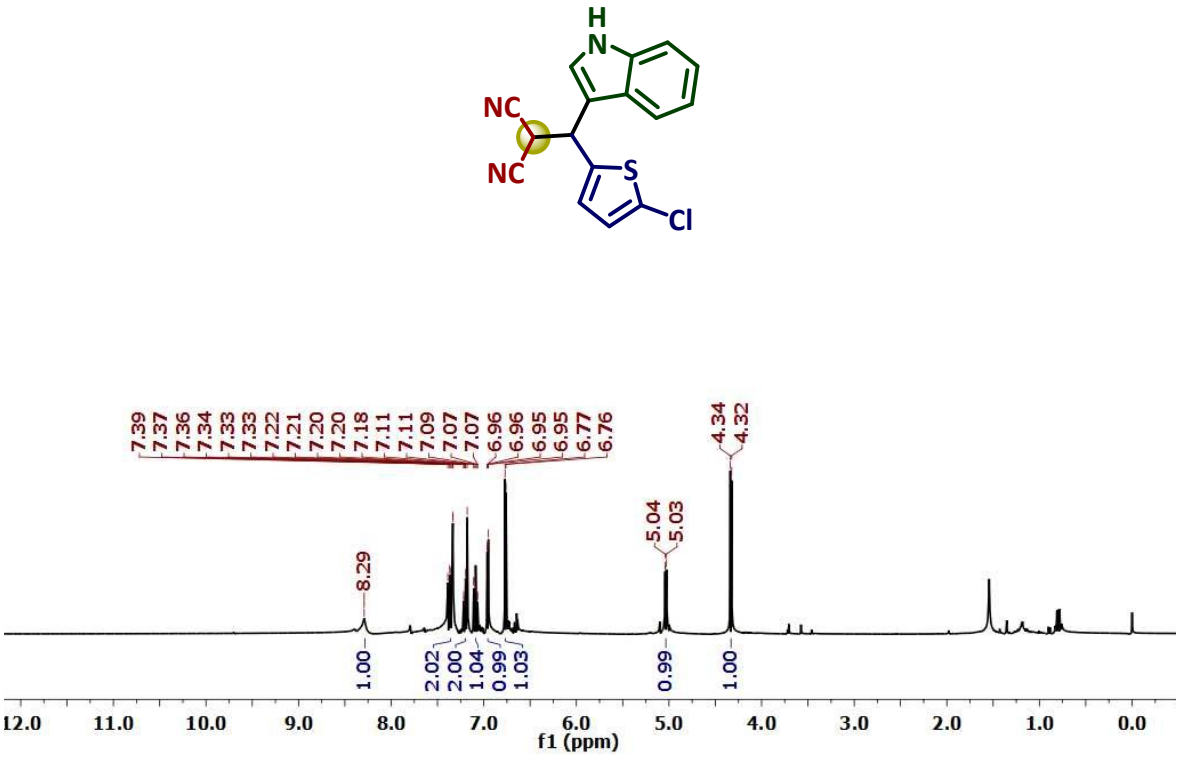

Figure S11: ^{1}H-NMR spectrum (400 MHz) in $CDCl_3$ of **5ac** compound

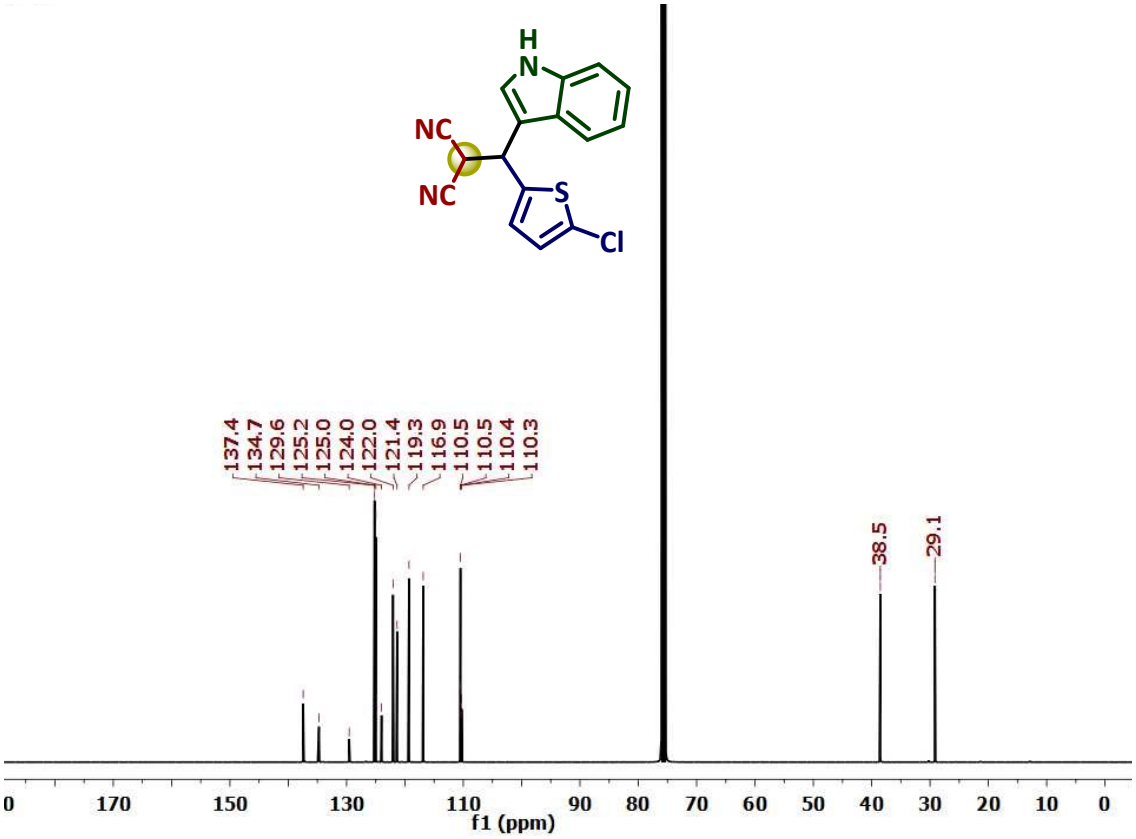

Figure S12: $^{13}C\{^{1}H\}$-NMR spectrum (101 MHz) in $CDCl_3$ of **5ac** compound

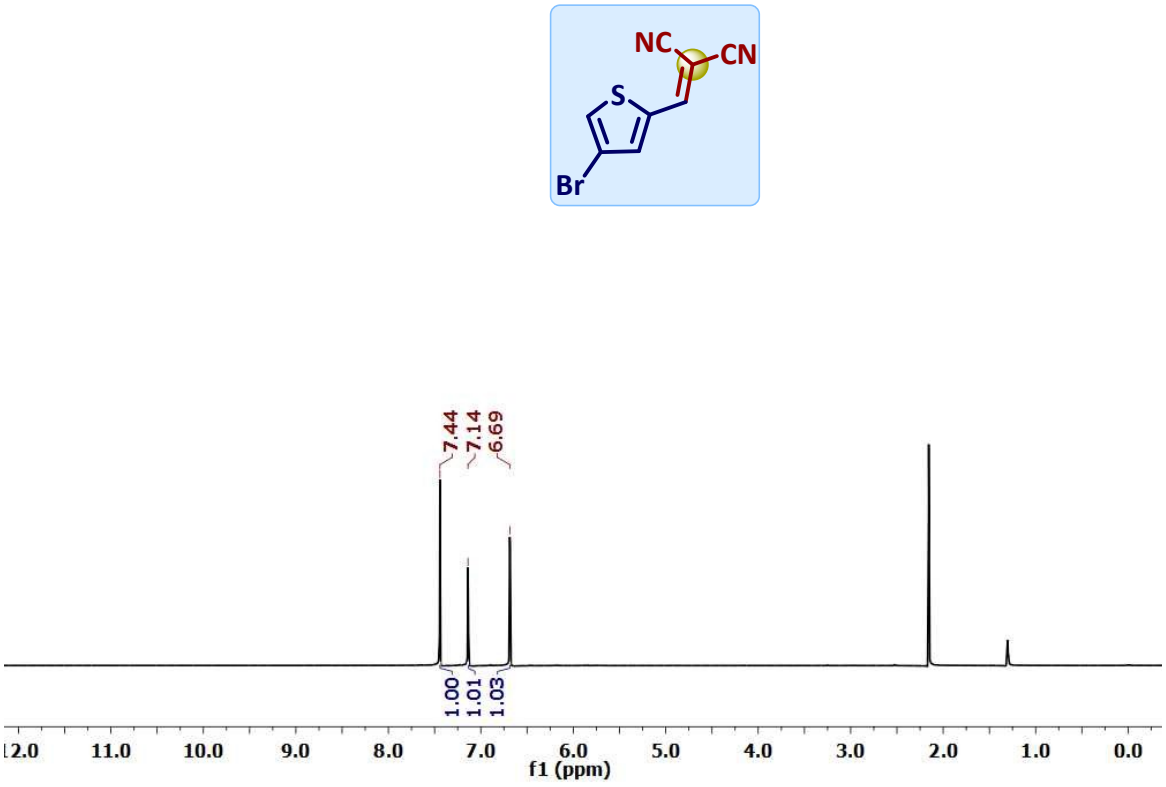

Figure S13: ^{1}H-NMR spectrum (400 MHz) in DMSO-d_6 of **3d** compound

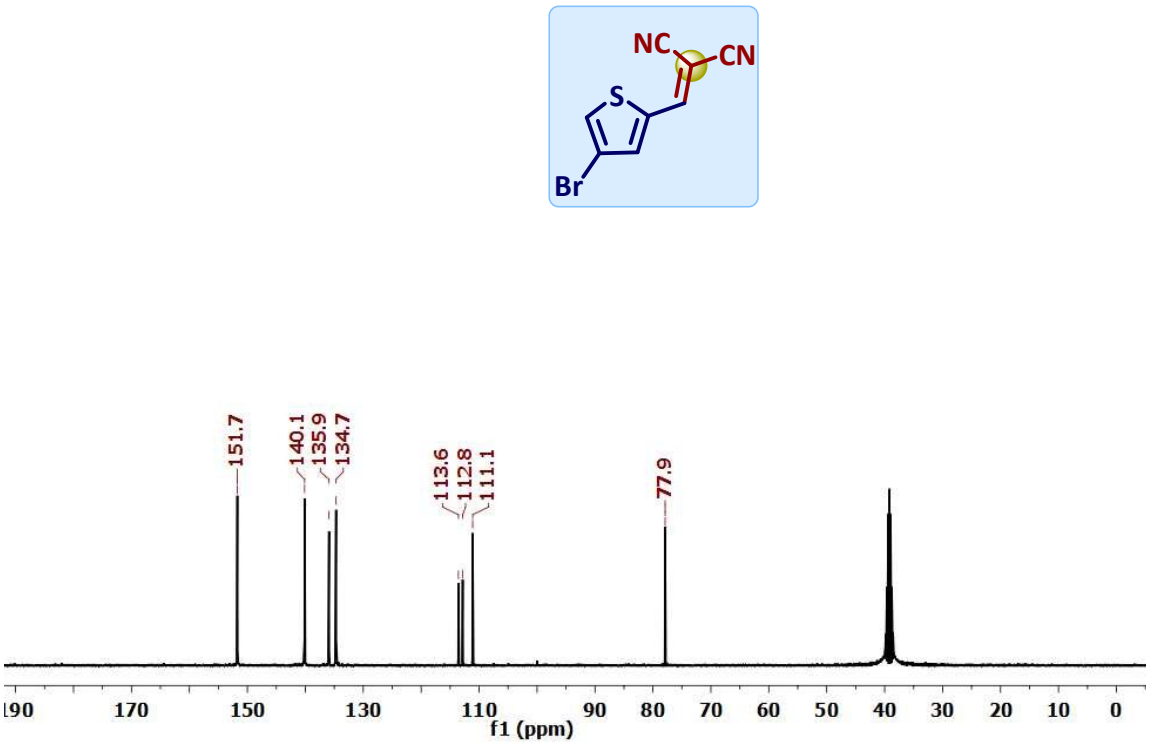

Figure S14: $^{13}C\{^{1}H\}$-NMR spectrum (101 MHz) in DMSO-d_6 of **3d** compound

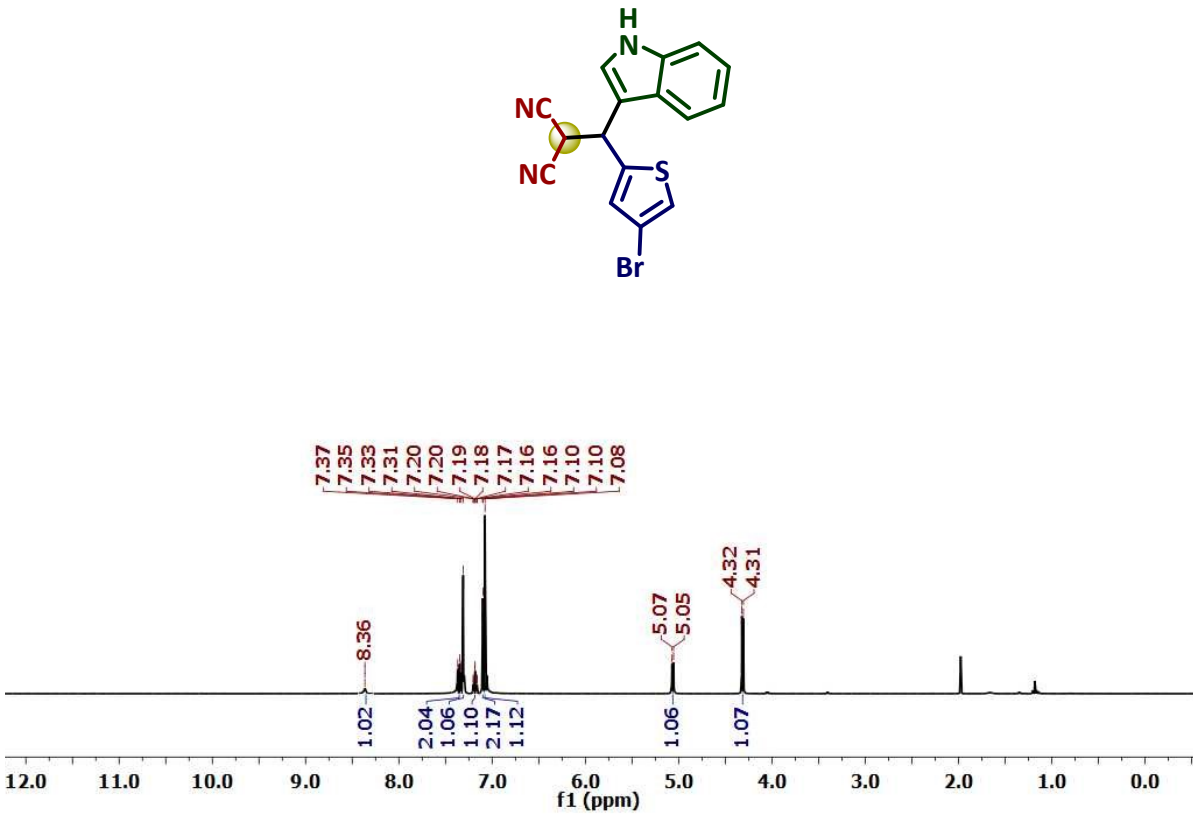

Figure S15: ^{1}H-NMR spectrum (400 MHz) in $CDCl_3$ of **5ad** compound

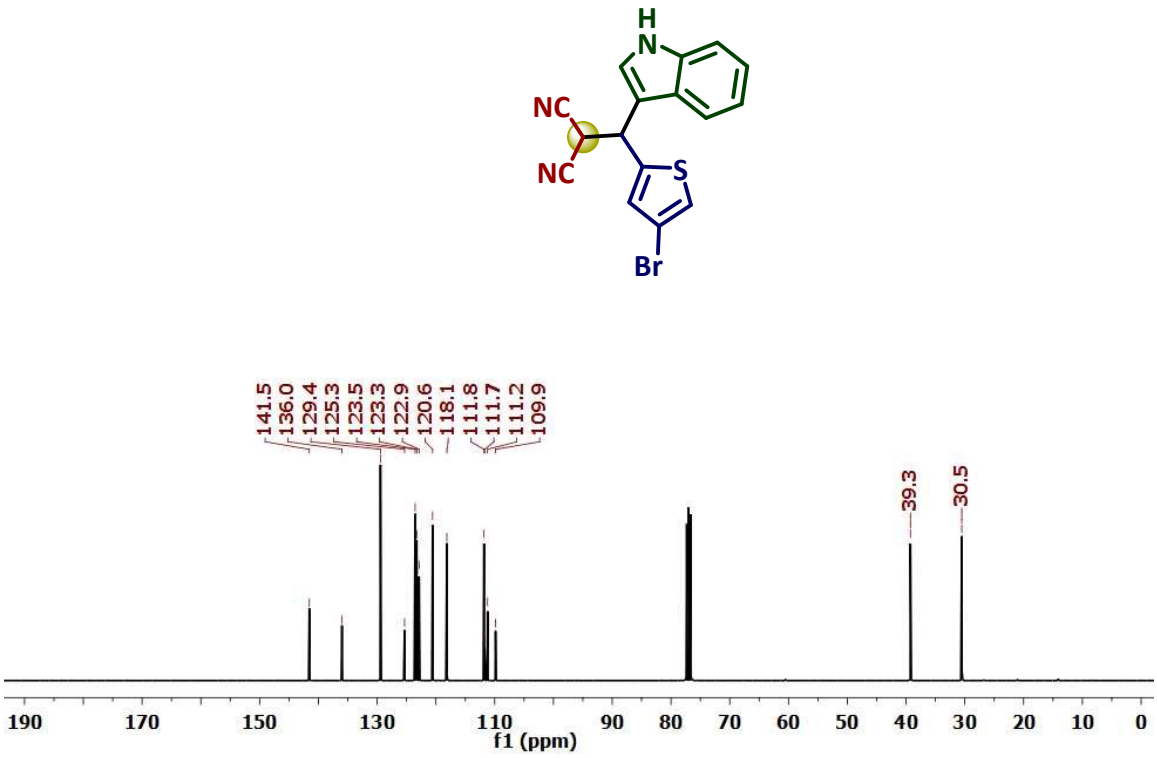

Figure S16: $^{13}C\{^{1}H\}$-NMR spectrum (101 MHz) in $CDCl_3$ of **5ad** compound

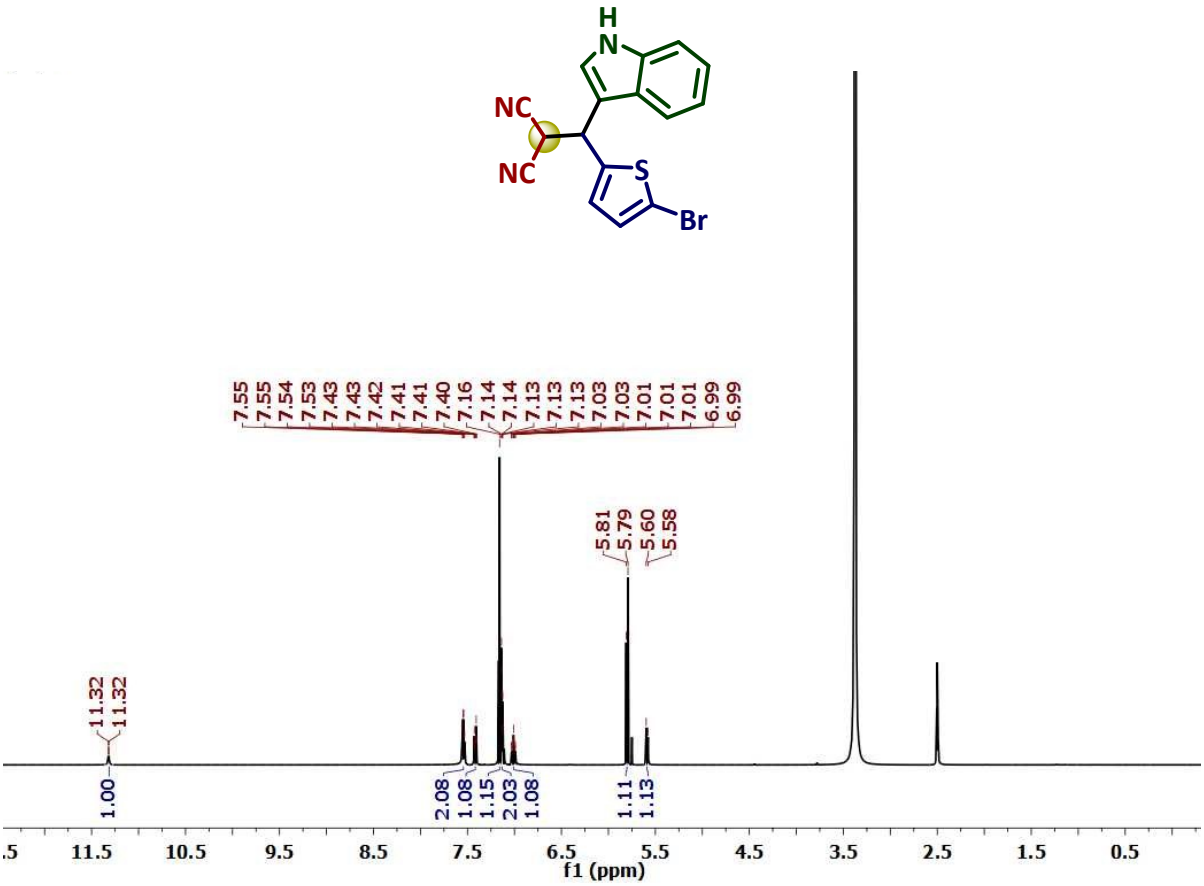

Figure S17: ^{1}H-NMR spectrum (400 MHz) in DMSO-d_6 of **5ae** compound

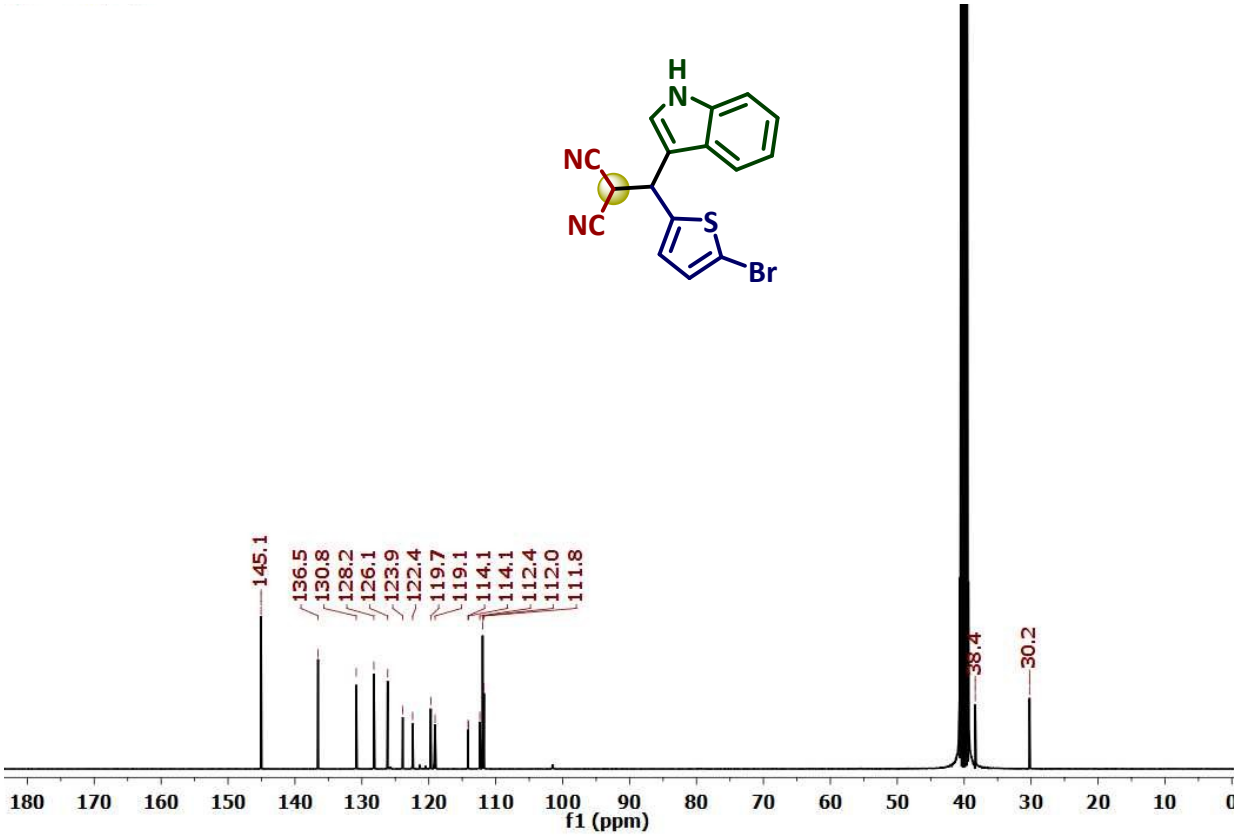

Figure S18: $^{13}C\{^{1}H\}$-NMR spectrum (101 MHz) in DMSO-d_6 of **5ae** compound

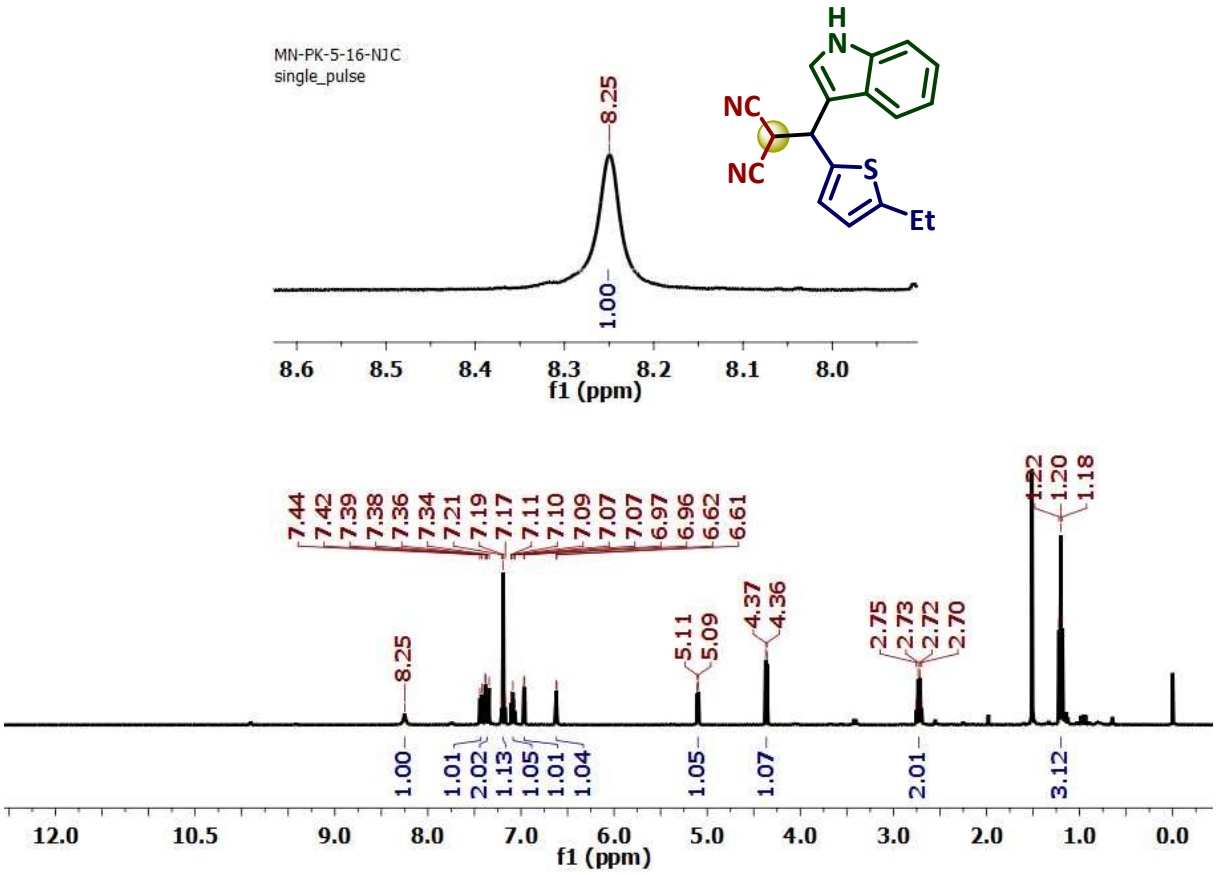

Figure S19: ^{1}H-NMR spectrum (400 MHz) in $CDCl_3$ of **5af** compound

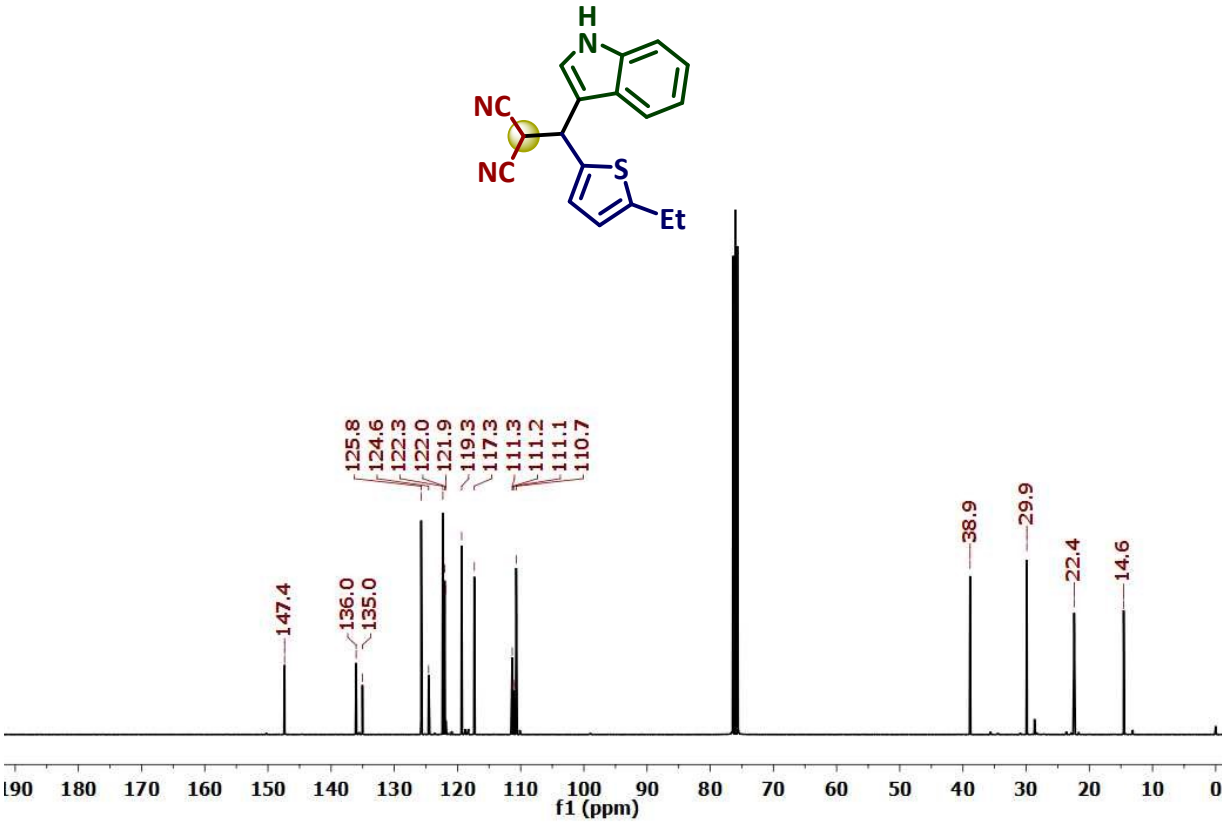

Figure S20: $^{13}C\{^{1}H\}$-NMR spectrum (101 MHz) in $CDCl_3$ of **5af** compound

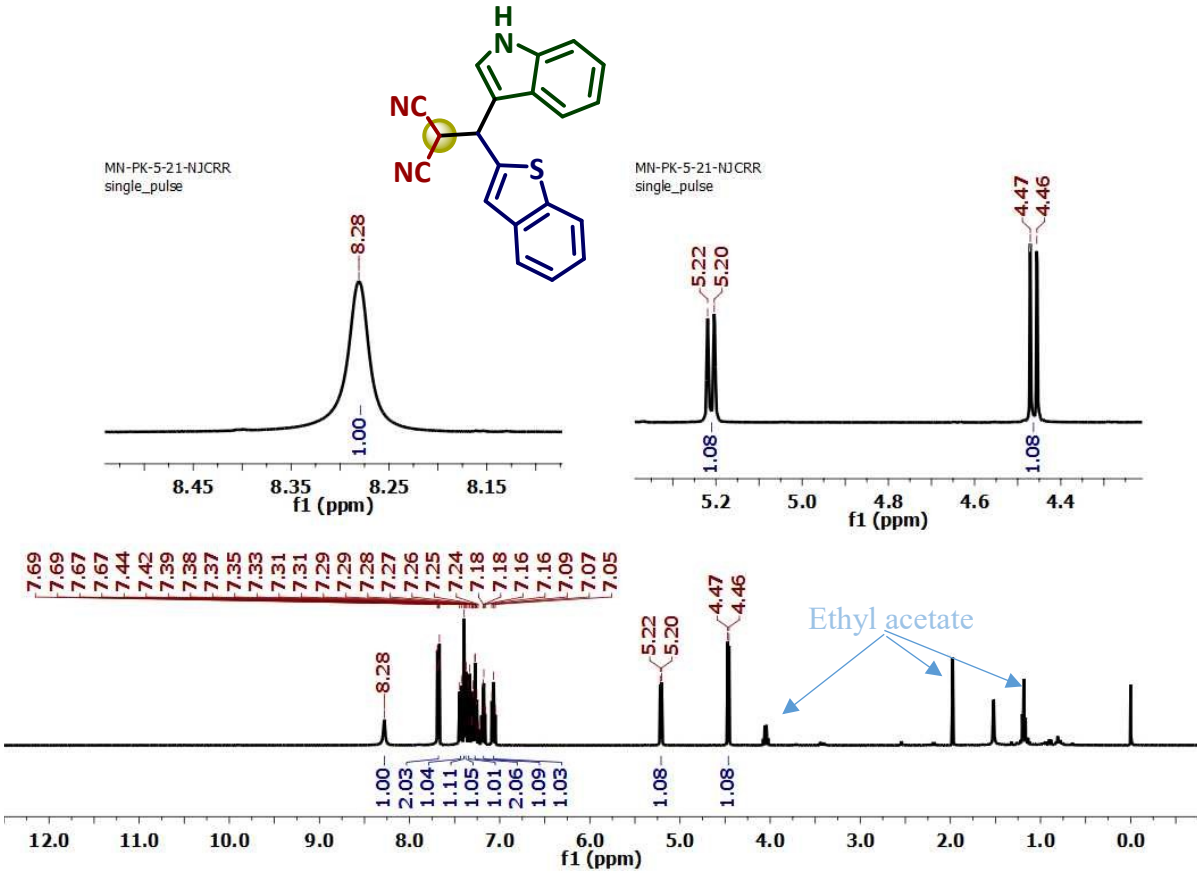

Figure S21: ^{1}H-NMR spectrum (400 MHz) in $CDCl_3$ of **5ag** compound

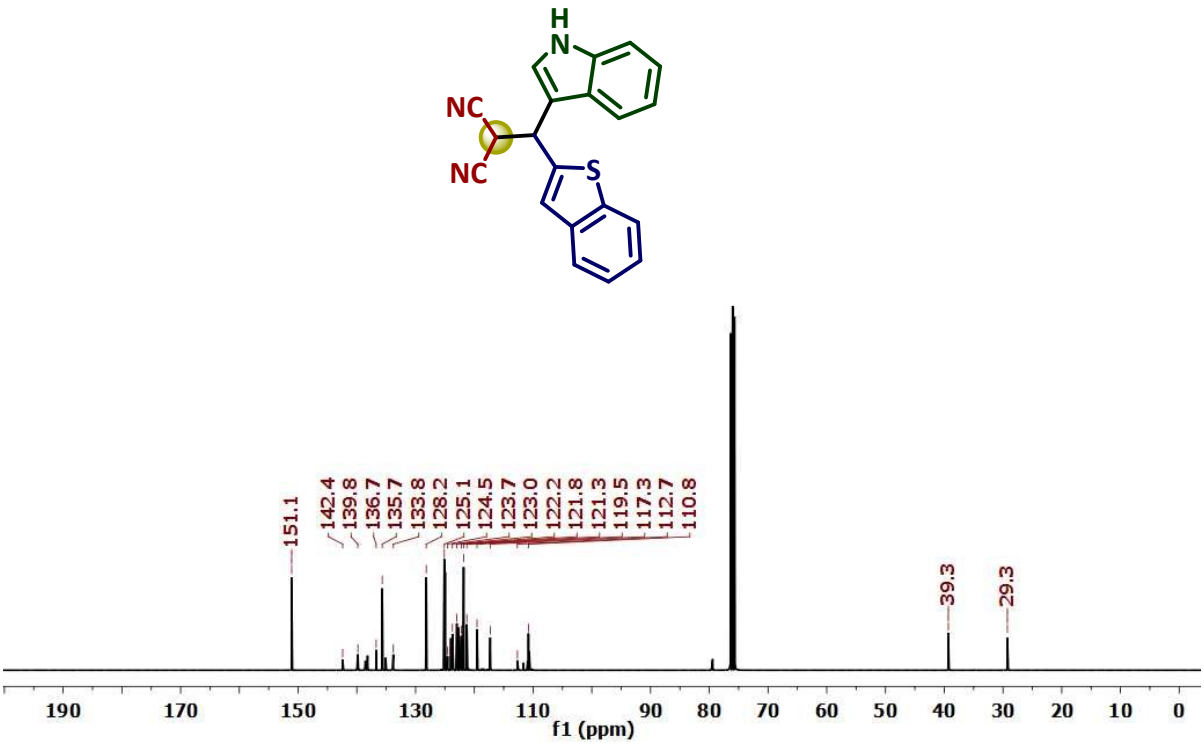

Figure S22: $^{13}C\{^{1}H\}$-NMR spectrum (101 MHz) in $CDCl_3$ of **5ag** compound

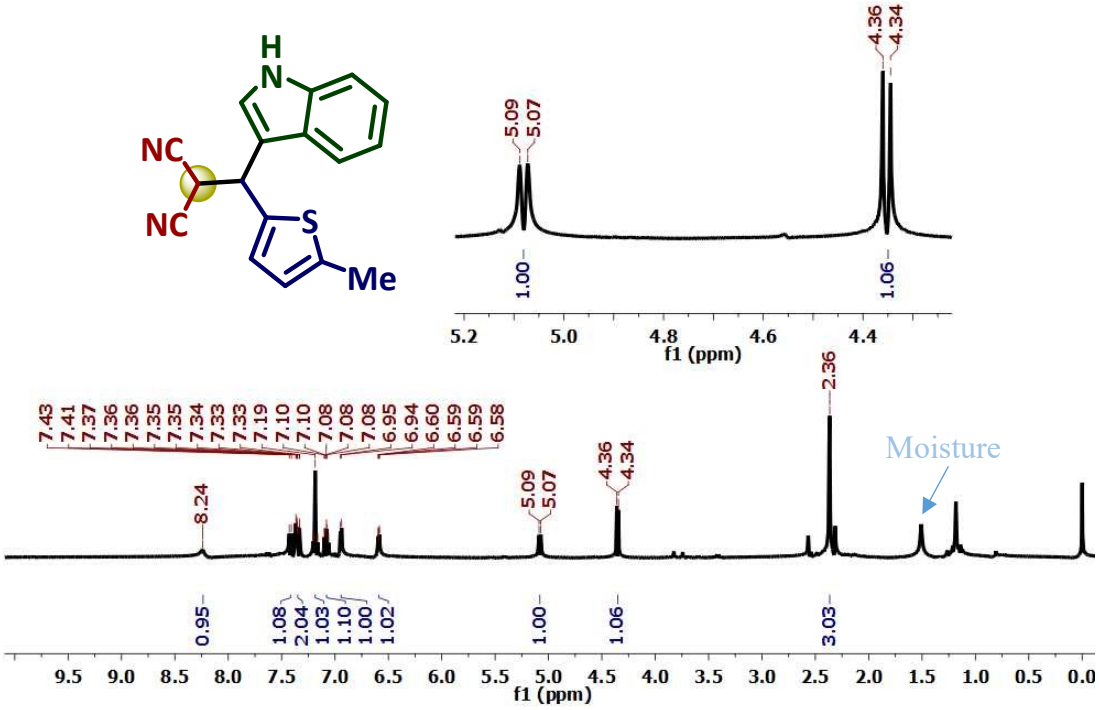

Figure S23: ^{1}H-NMR spectrum (400 MHz) in $CDCl_3$ of **5ah** compound

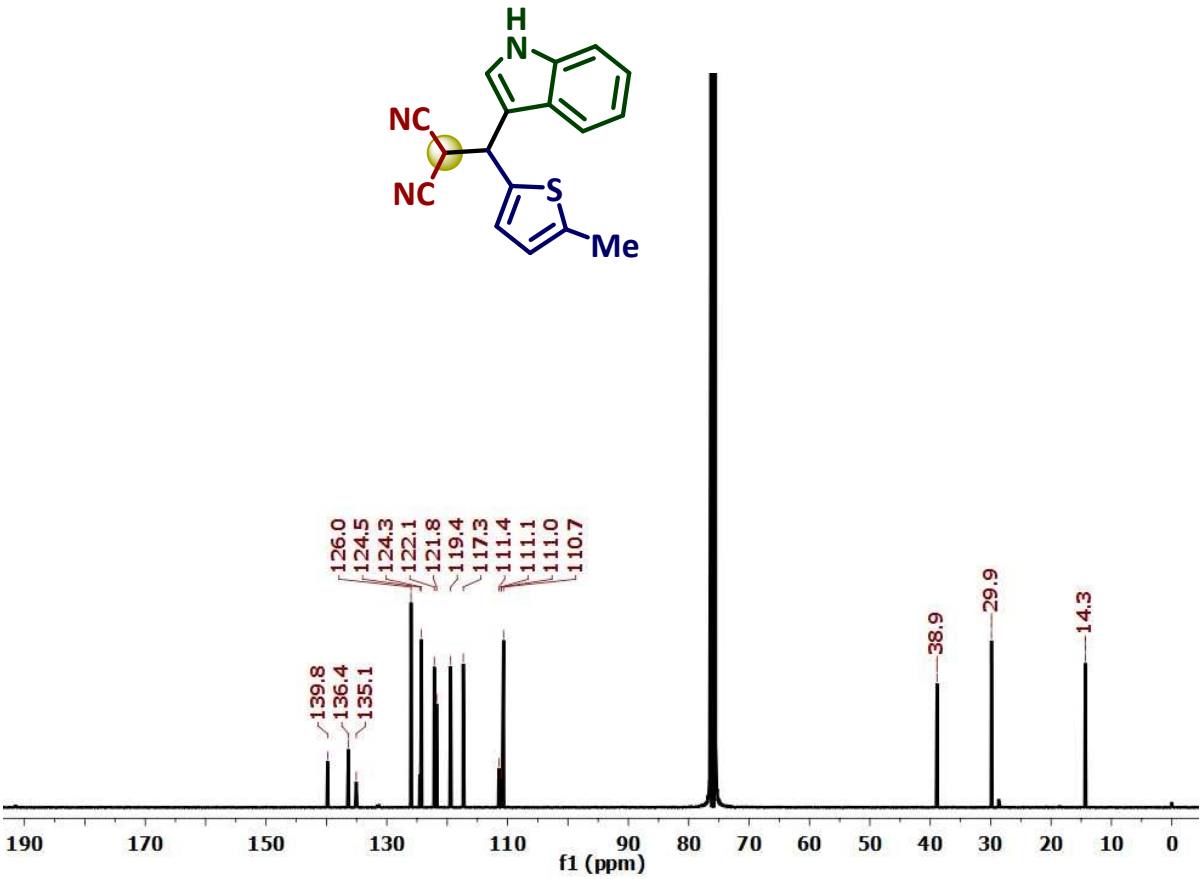

Figure S24: $^{13}C\{^{1}H\}$-NMR spectrum (101 MHz) in $CDCl_3$ of **5ah** compound

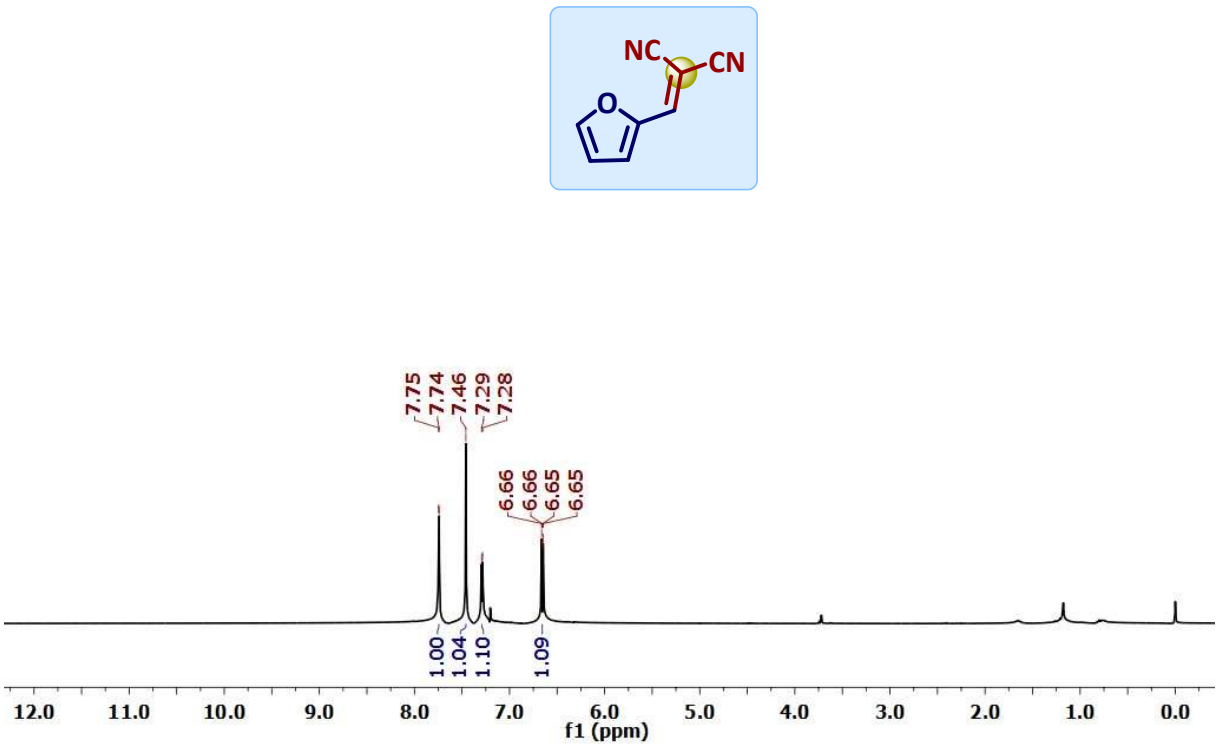

Figure S25: ^{1}H-NMR spectrum (400 MHz) in $CDCl_3$ of **3i** compound

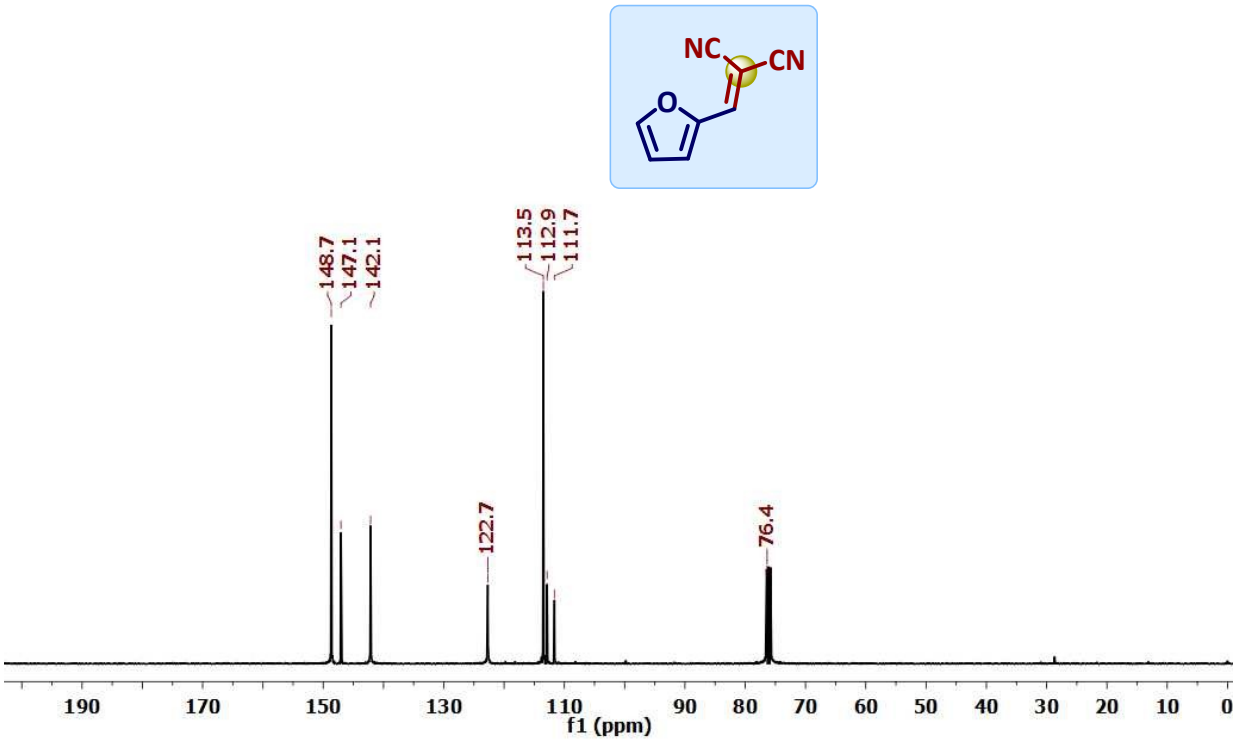

Figure S26: $^{13}C\{^{1}H\}$-NMR spectrum (101 MHz) in $CDCl_3$ of **3i** compound

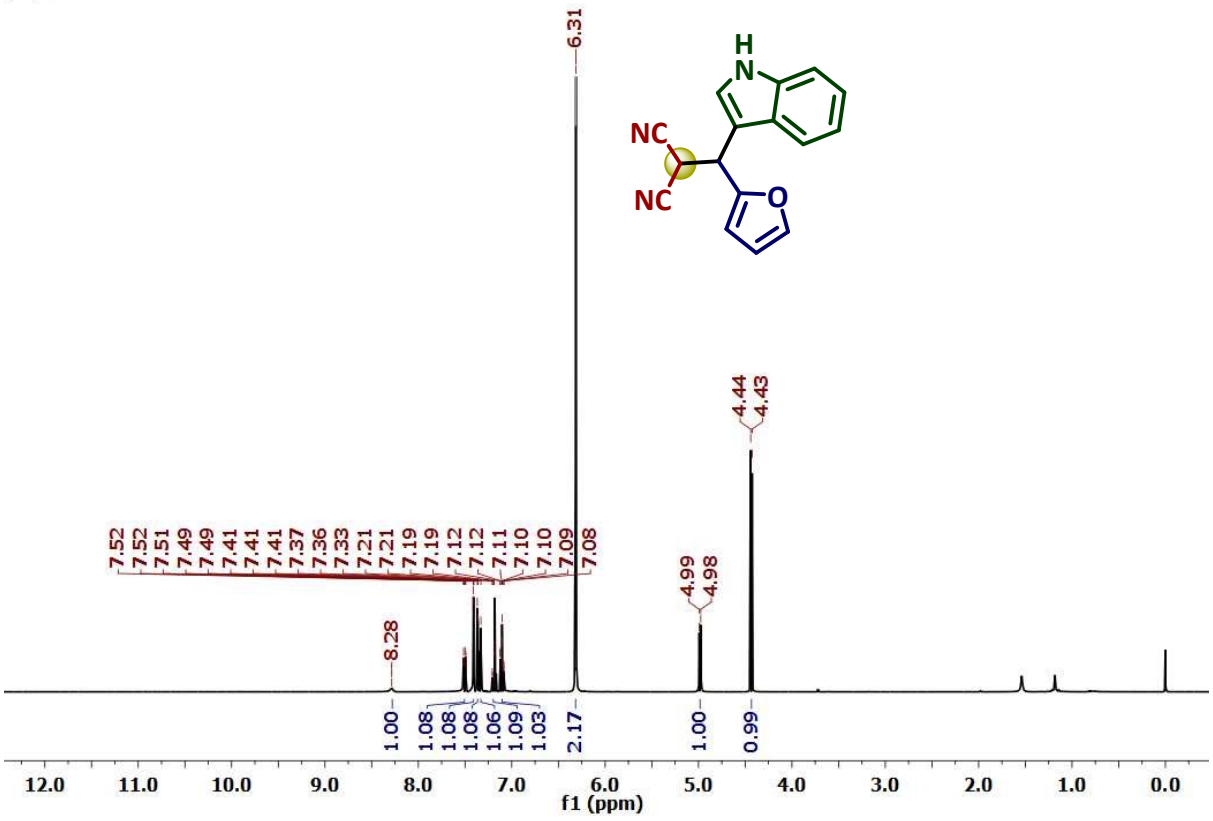

Figure S27: ^{1}H-NMR spectrum (400 MHz) in $CDCl_3$ of **5ai** compound

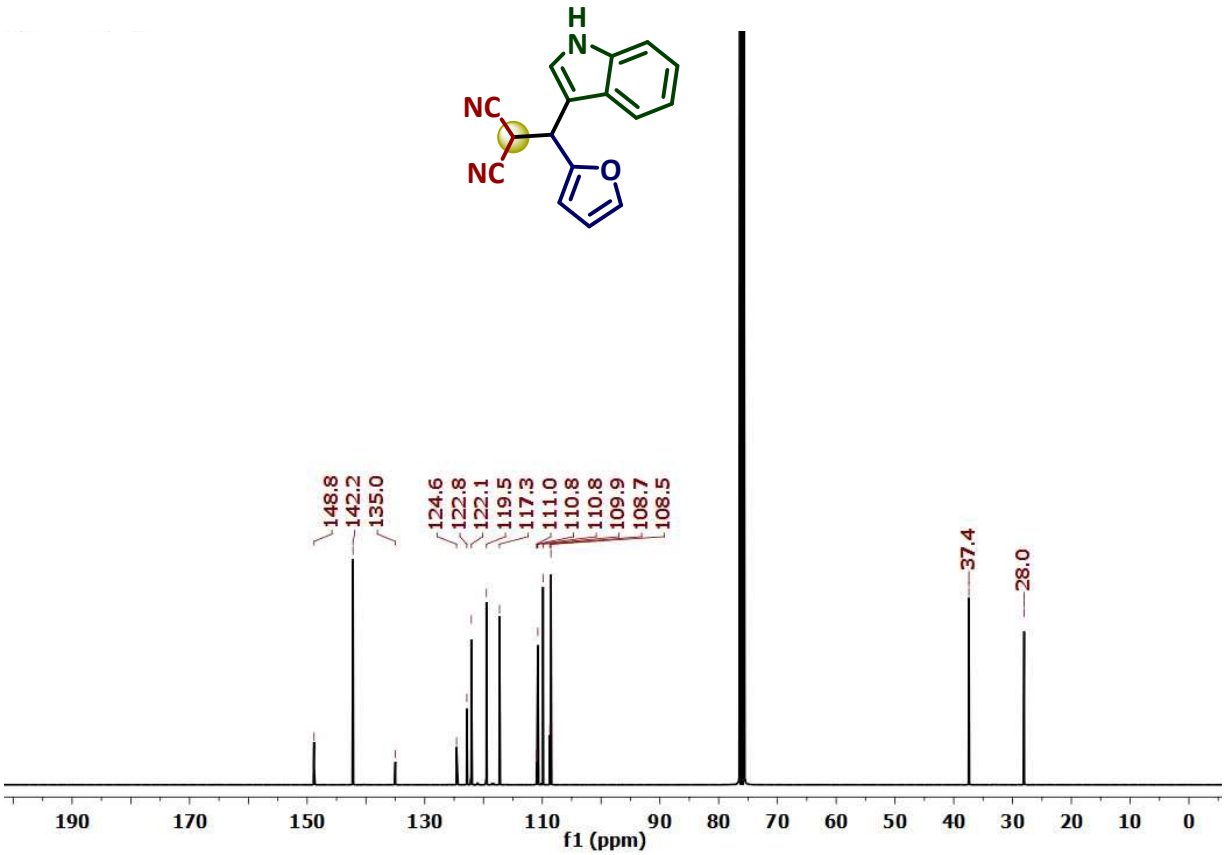

Figure S28: $^{13}C\{^{1}H\}$-NMR spectrum (101 MHz) in $CDCl_3$ of **5ai** compound

9. Spectral Data (^{1}H, ^{13}C{^{1}H}-NMR) of the Compound from Control Experiment (6aa)

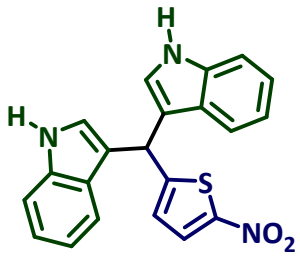

3,3'-((5-nitrothiophen-2-yl)methylene)bis(1H-indole) (6aa)[12,13]

Brown liquid; Yield 75 %

^{1}H-NMR (400 MHz, $CDCl_3$) δ 8.01 (s, 2H, br), 7.65 (d, *J* = 4.4 Hz, 1H), 7.35 (d, *J* = 8.8 Hz, 2H), 7.28 (d, *J* = 8.8 Hz, 2H), 7.15-7.10 (m, 2H), 7.01-6.96 (m, 2H), 6.79-6.73 (m, 3H), 6.02 (s, 1H) ppm. **^{13}C{^{1}H}-NMR (101 MHz, $CDCl_3$)** δ 159.1, 149.6, 136.4, 128.7, 126.1, 124.8, 123.2, 122.3, 119.6, 119.1, 117.3, 111.3, 36.1 ppm.

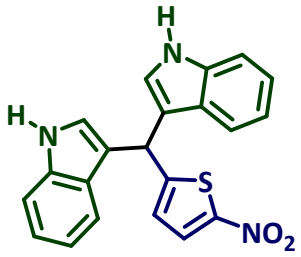

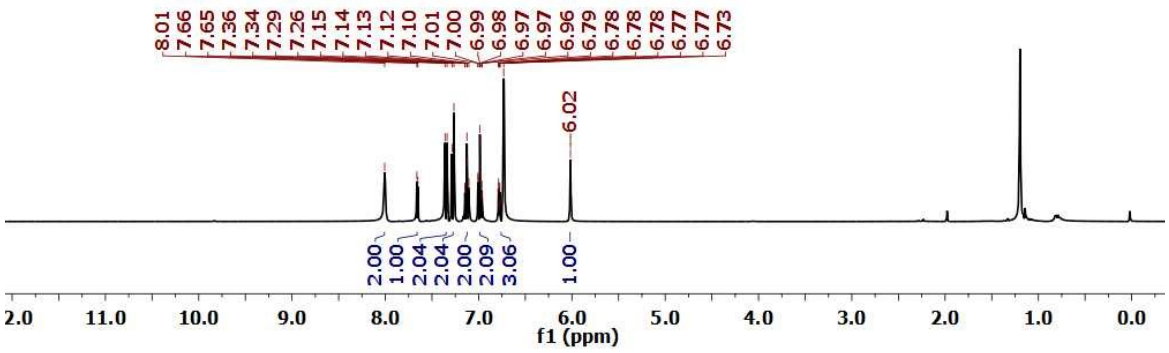

Figure S29: ^{1}H-NMR spectrum (400 MHz) in $CDCl_3$ of **6aa** compound

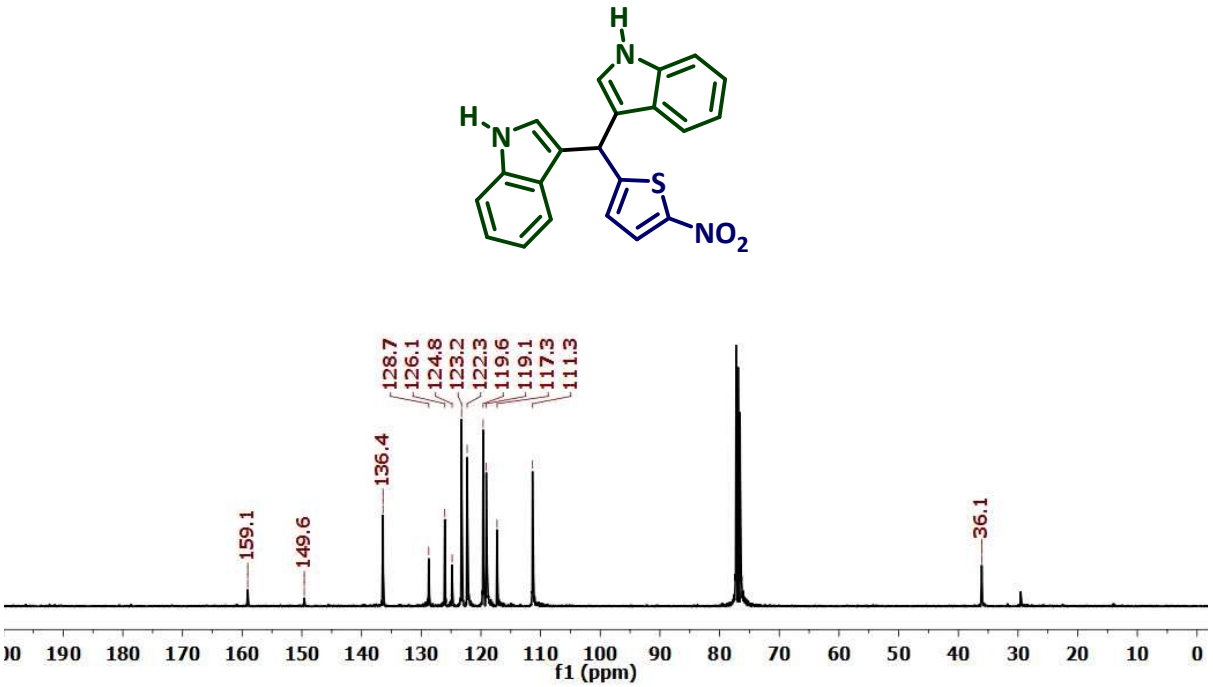

Figure S30: $^{13}C\{^{1}H\}$-NMR spectrum (101 MHz) in $CDCl_3$ of **6aa** compound

10. References

(1) Ma, P.; Wang, Y.; Wang, J. Copper-Catalyzed Three-Component Tandem Cyclization for One- Pot Synthesis of Indole-Benzofuran Bis-Heterocycles. **2024**. https://doi.org/10.1021/acs.joc.4c01680.

(2) Qu, Y.; Ke, F.; Zhou, L.; Li, Z.; Xiang, H.; Wu, D.; Zhou, X. Synthesis of 3-Indole Derivatives by Copper Sulfonato Salen Catalyzed Three-Component Reactions in Water. *Chem. Commun.* **2011**, *47* (13), 3912–3914. https://doi.org/10.1039/c0cc05695b.

(3) Anselmo, D.; Escudero-Adán, E. C.; Martínez Belmonte, M.; Kleij, A. W. Zn-Mediated Synthesis of 3-Substituted Indoles Using a Three-Component Reaction Approach. *Eur. J. Inorg. Chem.* **2012**, No. 29, 4694–4700. https://doi.org/10.1002/ejic.201200150.

(4) Singh, N.; Allam, B. K.; Raghuvanshi, D. S.; Singh, K. N. An Efficient Tetrabutylammonium Fluoride (TBAF)-Catalyzed Three-Component Synthesis of 3-Substituted Indole Derivatives under Solvent-Free Conditions. *Adv. Synth. Catal.* **2013**, *355* (9), 1840–1848. https://doi.org/10.1002/adsc.201300162.

(5) Wang, L.; Huang, M.; Zhu, X.; Wan, Y. Polyethylene Glycol (PEG-200)-Promoted Sustainable One-Pot Three-Component Synthesis of 3-Indole Derivatives in Water. *Appl. Catal. A Gen.* **2013**, *454*, 160–163. https://doi.org/10.1016/j.apcata.2012.12.008.

(6) Rajesh, U. C.; Wang, J.; Prescott, S.; Tsuzuki, T.; Rawat, D. S. RGO/ZnO Nanocomposite: An Efficient, Sustainable, Heterogeneous, Amphiphilic Catalyst for Synthesis of 3-Substituted Indoles in Water. *ACS Sustain. Chem. Eng.* **2015**, *3* (1), 9–18. https://doi.org/10.1021/sc500594w.

(7) He, Y.-H.; Cao, J.-F.; Li, R.; Xiang, Y.; Yang, D.-C.; Guan, Z. L-Proline-Catalyzed Multicomponent Synthesis of 3-Indole Derivatives. *Tetrahedron* **2015**, *71* (49), 9299–9306. https://doi.org/https://doi.org/10.1016/j.tet.2015.10.027.

(8) Prasad, A. N.; Braga, F. C.; Lopes, R. da S.; Casagrande, G. A.; de Lima, D. P.; Beatriz, A. Cu(I)-Phosphine Complex: An Efficient Catalyst for Synthesis of 3-Indole Derivatives through One-Pot MCR under Mild Conditions. *Synth. Commun.* **2018**, *48* (1), 104–114. https://doi.org/10.1080/00397911.2017.1394467.

(9) Wu, Y.; Li, J.; Sun, J.; Wang, Y.; Liu, J.; Cheng, H. Synthesis of 3-Substituted Indoles by Yonemitsu Three-Component Reactions Accelerated in Microdroplet/Thin Film. *J. Org. Chem.* **2024**. https://doi.org/10.1021/acs.joc.4c02395.

(10) Au, J. L.; Kumar, R. R.; Li, D.; Wientjes, M. G. Kinetics of Hallmark Biochemical Changes in Paclitaxel-Induced Apoptosis. *AAPS PharmSci* **1999**, *1* (3), E8. https://doi.org/10.1208/ps010308.

(11) Zengin, N.; Burhan, H.; Şavk, A.; Göksu, H.; Şen, F. Synthesis of Benzylidenemalononitrile by Knoevenagel Condensation through Monodisperse Carbon Nanotube-Based NiCu Nanohybrids. *Sci. Rep.* **2020**, *10* (1), 1–7. https://doi.org/10.1038/s41598-020-69764-8.

(12) Sarva, S.; Harinath, J. S.; Sthanikam, S. P.; Ethiraj, S.; Vaithiyalingam, M.; Cirandur, S. R. Synthesis, Antibacterial and Anti-Inflammatory Activity of Bis(Indolyl)Methanes. *Chinese Chem. Lett.* **2016**, *27* (1), 16–20. https://doi.org/10.1016/j.cclet.2015.08.012.

(13) Kumar, P.; Kumar, G.; Tomar, V.; Nemiwal, M. Sustainable Synthesis of Bis(Indolyl)Methane Scaffolds Catalyzed by CuO Nanoparticles Immobilized with Triethylammonium Bistriflimide Ionic Liquid. *New J. Chem.* **2025**. https://doi.org/10.1039/d5nj03257a.